Impaired fatty acid import or catabolism in macrophages restricts intracellular growth of *Mycobacterium tuberculosis*

Nelson V. Simwela[1], Eleni Jaecklein [2], Christopher M. Sassetti[2], David G. Russell[1]*

1. Department of Microbiology and Immunology, College of Veterinary Medicine, Cornell University, Ithaca, New York, USA
2. Department of Microbiology, UMass Chan Medical School, Worcester, Massachusetts, USA

*Correspondence: dgr8@cornell.edu

Abstract

Mycobacterium tuberculosis (*Mtb*) infection of macrophages reprograms cellular metabolism to promote lipid retention. While it is clearly known that intracellular *Mtb* utilize host derived lipids to maintain infection, the role of macrophage lipid processing on the bacteria's ability to access the intracellular lipid pool remains undefined. We utilized a CRISPR-Cas9 genetic approach to assess the impact of sequential steps in fatty acid metabolism on the growth of intracellular *Mtb*. Our analyzes demonstrate that macrophages which cannot either import, store or catabolize fatty acids restrict *Mtb* growth by both common and divergent anti-microbial mechanisms, including increased glycolysis, increased oxidative stress, production of pro-inflammatory cytokines, enhanced autophagy and nutrient limitation. We also show that impaired macrophage lipid droplet biogenesis is restrictive to *Mtb* replication, but increased induction of the same fails to rescue *Mtb* growth. Our work expands our understanding of how host fatty acid homeostasis impacts *Mtb* growth in the macrophage.

Key words: Macrophages, *Mycobacterium tuberculosis*, lipid metabolism, CRISPR-Cas9, nutritional immunity

59 **Introduction**

60 *Mycobacterium tuberculosis* (*Mtb*), the causative agent of tuberculosis (TB), has caused disease
61 and death in humans for centuries (WHO, 2023). *Mtb* primarily infects macrophages in the lung
62 (Cohen et al., 2018; Wolf et al., 2007) wherein the bacterium relies on host derived fatty acids
63 and cholesterol for synthesis of its lipid rich cell wall, and to produce energy and virulence
64 factors (Peyron et al., 2008; Russell et al., 2009; Singh et al., 2012; Daniel et al., 2011; Muñoz-
65 Elías and McKinney, 2005; Pandey and Sassetti, 2008; Brzostek et al., 2009). Within the lung
66 microenvironment, resident alveolar macrophages preferentially oxidize fatty acids and are
67 more permissive to *Mtb* growth while recruited interstitial macrophages are more glycolytic and
68 restrictive of *Mtb* replication (Huang et al., 2018; Pisu et al., 2020; Pisu et al., 2021). Globally,
69 *Mtb* infection modifies macrophage metabolism in a manner that enhances its survival. *Mtb*
70 infected macrophages shift their mitochondrial substrate preference to exogenous fatty acids
71 which drives the formation of foamy macrophages that are laden with cytosolic lipid droplets
72 (Peyron et al., 2008; Russell et al., 2009; Cumming et al., 2018; Singh et al., 2012; Podinovskaia
73 et al., 2013). Foamy macrophages are found in abundance in the central and inner layers of
74 granulomas, a common histopathological feature of human TB (Russell et al., 2009; Kim et al.,
75 2010). Interference with key regulators of lipid homeostasis, such as the miR-33 and the
76 transcription factors peroxisome proliferator-activated receptor α (PPARα) and PPAR-γ enhances
77 macrophage control of *Mtb* (Kim et al., 2017; Almeida et al., 2009; Ouimet et al., 2016).
78 Moreover, compounds which modulate lipid metabolism such as the anti-diabetic drug
79 metformin and some cholesterol lowering drugs are under investigation for host directed
80 therapeutics (HDTs) against *Mtb* (Parihar et al., 2014; Singhal et al., 2014). Although the
81 dependence of intracellular *Mtb* on host fatty acids and cholesterol is well documented
82 (Wilburn et al., 2018), the impact of specific aspects of macrophage lipid metabolism on the
83 bacteria remains opaque. In *Mtb* infected foamy macrophages, bacteria containing phagosomes
84 are found in close apposition to intracellular lipid droplets (Peyron et al., 2008). It is believed
85 that the bacterial induction of a foamy macrophage phenotype in host cells results in a steady
86 supply of lipids that addresses the bacteria's nutritional requirements (Peyron et al., 2008;
87 Russell et al., 2009; Singh et al., 2012; Daniel et al., 2011). In fact, intracellular *Mtb* has been

88 shown to import fatty acids from host lipid droplet derived triacylglycerols (Daniel et al., 2011).
89 However, other studies indicate that macrophage lipid droplet formation in response to *Mtb*
90 infection can lead to the induction of a protective, anti-microbial response (Knight et al., 2018).
91 *Mtb* appears unable to acquire host lipids when lipid droplets are induced by stimulation with
92 interferon gamma (IFN-γ) (Knight et al., 2018). Moreover, there is some evidence that lipid
93 droplets can be sites for the production of host protective pro-inflammatory eicosanoids (Knight
94 et al., 2018; Daniel et al., 2011). Lipid droplets can also act as innate immune hubs against
95 intracellular bacterial pathogens by clustering anti-bacterial proteins (Bosch et al., 2020).
96 Inhibition of macrophage fatty acid oxidation by knocking out mitochondrial carnitine palmitoyl
97 transferase 2 (CPT2) or using chemical inhibitors of CPT2 also restrict intracellular growth of *Mtb*
98 (Chandra et al., 2020; Huang et al., 2018). These data demonstrate that modulation of the
99 different stages in lipid metabolism inside *Mtb* infected macrophages can result in conflicting
100 outcomes.
101
102 We carried out a candidate-based, CRISPR mediated knockout of lipid import and metabolism
103 genes in macrophages to determine their roles in intracellular growth of *Mtb*. By targeting
104 genes involved in fatty acid import, sequestration, and metabolism in Hoxb8 derived
105 conditionally immortalized murine macrophages (Kiritsy et al., 2021), we show that impairing
106 lipid homeostasis in macrophages at different steps in the process negatively impacts the
107 growth of intracellular *Mtb*, albeit to differing degrees. The impact on *Mtb* growth in the
108 mutant macrophages was mediated through different mechanisms despite some common anti-
109 microbial effectors. *Mtb* infected macrophages deficient in the import of long chain fatty acids
110 increased production of pro-inflammatory markers such as interleukin 1β (IL-1β). In contrast,
111 ablation of lipid droplet biogenesis and fatty acid oxidation increased production of reactive
112 oxygen species and limited the bacteria's access to nutrients. We also found that suppression of
113 *Mtb* growth in macrophages that are unable to produce lipid droplets could not be rescued by
114 exogeneous addition of fatty acids indicating that this is not purely nutritional restriction. Our
115 data indicate that interference of lipid metabolism in macrophages leads to suppression of *Mtb*
116 growth via multiple routes.

117

118

119 **Results**

120 **Knockout of fatty acid import and metabolism genes restricts *Mtb* growth in macrophages**

121 To apply a holistic approach to assessing the role(s) of fatty acid metabolism on the intracellular
122 growth of *Mtb*, we used a CRISPR genetic approach to knockout genes involved in lipid import
123 (CD36, FATP1), lipid droplet formation (PLIN2) and fatty acid oxidation (CPT1A, CPT2) in murine
124 primary macrophages (Figure 1A). Deletion of CD36 or CPT2 in mouse macrophages has been
125 shown to impair intracellular growth of *Mtb* (Hawkes et al., 2010; Chandra et al., 2020). But the
126 role of specialized long chain fatty acid transporters (FATP1-6) on *Mtb* growth in macrophages is
127 uncharacterized. FATP1 and FATP4 are the most abundant fatty acid transporter isoforms in
128 macrophages (Nishiyama et al., 2018). PLIN2, or adipophilin, is known to be required for lipid
129 droplet formation (Paul et al., 2008; Larigauderie et al., 2004). Five isoforms of mammalian
130 perilipins (PLIN) are involved in lipid droplet biogenesis amongst which PLIN2 is the dominant
131 isoform expressed in macrophages (Knight et al., 2018). However, macrophages derived from
132 PLIN2$^{-/-}$ mice show no defects in production of lipid droplets nor do they impair intracellular
133 growth of *Mtb* (Knight et al., 2018). We targeted each of these genes with at least two sgRNAs
134 in Hoxb8 Cas9^{+} conditionally immortalized myeloid progenitors (Kiritsy et al., 2021) to generate
135 a panel of mutants that were deficient in the following candidates of interest; FATP1$^{-/-}$, PLIN2$^{-/-}$,
136 CD36$^{-/-}$, CPT1A$^{-/-}$ and CPT2$^{-/-}$. Each individual sgRNA achieved >85% CRISPR-mediated deletion
137 efficiency for all the five genes, as analyzed by the Inference for CRISPR Edits (ICE) tool (Conant
138 et al., 2022) (Supplementary file 1). We verified the protein knockout phenotypes by flow
139 cytometry and western blot analysis of differentiated macrophages derived from the CRISPR
140 deleted Hoxb8 myeloid precursors (Figure 1 - figure supplement 1).

141 To confirm certain knockout phenotypes functionally, we checked lipid droplet
142 biogenesis in PLIN2$^{-/-}$ macrophages in comparison to macrophages transduced with a non-
143 targeting scramble sgRNA by confocal microscopy of BODIPY stained cells. Cells were cultured
144 for 24 hours in the presence of exogenous oleate to enhance the formation of lipid droplets
145 (Listenberger and Brown, 2007). We observed a complete absence of lipid droplet formation in

146 PLIN2$^{-/-}$ macrophages as compared to controls (Figure 1 - figure supplement 2A). This is contrary
147 to previous observations in macrophages derived from PLIN2 knockout mice which were
148 reported to have no defect in lipid droplet formation (Knight et al., 2018). We also assessed the
149 ability of CPT2$^{-/-}$ macrophages to oxidize fatty acids using the Agilent Seahorse XF Palmitate
150 Oxidation Stress Test. Scrambled sgRNA and CPT2$^{-/-}$ macrophages were cultured in substrate
151 limiting conditions and supplied with either bovine serum albumin (BSA) or BSA conjugated
152 palmitate. As shown in Figure 1 - figure supplement 2B, control macrophages were able to
153 utilize and oxidize palmitate in substrate limiting conditions indicated by a significant increase in
154 oxygen consumption rates (OCRs) in contrast to cells supplied with BSA alone. Addition of the
155 CPT1A inhibitor, etomoxir, inhibited the cell's ability to use palmitate in these conditions (Figure
156 1 - figure supplement 2B). CPT2 knockout in CPT2$^{-/-}$ macrophages impaired the cell's ability to
157 oxidize palmitate to a degree comparable to etomoxir treatment as evidenced by baseline OCRs
158 when compared to scrambled sgRNA control (Figure 1 - figure supplement 2C).
159 We then assessed the different knockout mutant macrophages in their ability to support
160 the intracellular growth of *Mtb*. We infected macrophages with *Mtb* Erdman at a multiplicity of
161 infection (MOI) of 0.4 and assessed intracellular bacterial growth rates by counting colony
162 forming units (CFUs) 5 days post infection. All the five mutant macrophages significantly
163 impaired *Mtb* growth rates when compared to scrambled sgRNA as assessed by CFUs counts on
164 day 5 (Figure 1B). PLIN2$^{-/-}$, FATP1$^{-/-}$ and CPT2$^{-/-}$ macrophages displayed the strongest growth
165 restriction phenotypes while CD36$^{-/-}$macrophages had a moderate, but significant, impact on
166 *Mtb* growth. In parallel, we quantified intracellular bacteria on day 0, 3 hours post infection
167 (Figure 1C), to ascertain that subsequent differences on day 5 were not due to disparities in
168 initial bacterial uptake. The moderate growth restriction phenotypes of CD36$^{-/-}$ macrophages
169 were consistent with previous findings which reported similar impact on *Mtb* and *M. marinum*
170 growth in macrophages derived from CD36$^{-/-}$ mice (Hawkes et al., 2010). Impaired growth of
171 *Mtb* in CPT1A$^{-/-}$ and CPT2$^{-/-}$ macrophages is also consistent with previous reports that genetic
172 and chemical inhibition of fatty acid oxidation is detrimental to the growth of *Mtb* within
173 macrophages (Huang et al., 2018; Chandra et al., 2020).
174

175

176 ***Mtb* infected macrophages with impaired fatty acid import and metabolism display altered**
177 **mitochondrial metabolism and elevated glycolysis.**

178 Impairment of fatty acids metabolism by FATP1 knockout in macrophages rewires their
179 substrate bias from fatty acids to glucose (Johnson et al., 2016). We reasoned that deletion of
180 genes required for downstream processing of lipids (Figure 1A) could also reprogram
181 macrophages and increase glycolysis which could, in part, explain bacterial growth restriction.
182 We analyzed the metabolic states of three knockout macrophages (FATP1$^{-/-}$, PLIN2$^{-/-}$ and CPT2$^{-/-}$)
183 in uninfected and *Mtb* infected conditions by monitoring oxygen consumption rates (OCR) and
184 extracellular acidification rates (ECARs) using the Agilent Mito and Glucose Stress Test kits. All
185 three mutant uninfected macrophages displayed reduced mitochondrial respiration as
186 evidenced by lower basal and spare respiratory capacity (SRC) when compared to scrambled
187 sgRNA controls (Figure 2 - figure supplement 1A, 1B). *Mtb* infection proportionally reduced
188 basal and SRC rates across all the mutant macrophages and scrambled controls (Figure 2A, 2B)
189 when compared to uninfected macrophages, which is consistent with previous findings
190 (Cumming et al., 2018). PLIN2$^{-/-}$ macrophages displayed the most marked reduction in
191 mitochondrial activity in both uninfected and infected conditions, while FATP1$^{-/-}$ macrophages
192 were the least affected (Figure 2A, Figure 2 - figure supplement 1A). As reported previously
193 (Johnson et al., 2016), uninfected FATP1$^{-/-}$ macrophages were more glycolytically active with
194 higher basal and spare glycolytic capacity (SGC) compared to scrambled controls (Figure 2 -
195 figure supplement 1C, 1D). Uninfected PLIN2$^{-/-}$ and CPT2$^{-/-}$ macrophages were also more
196 glycolytically active, but to a greater degree than FATP1$^{-/-}$ (Figure 2 - figure supplement 1C, 1D).
197 *Mtb* infection increased the glycolytic capacity of all the three mutant macrophages (Figure 2C,
198 2D). Overall, PLIN2$^{-/-}$ macrophages exhibited the highest glycolytic capacity (Figure 2C, Figure 2 -
199 figure supplement 1D). Our data indicates that impairment of fatty acid metabolism at different
200 steps significantly impacts mitochondrial respiration and reprograms cells towards glycolysis.
201 Increased glycolytic flux in macrophages has been linked to the control of intracellular *Mtb*
202 growth (Gleeson et al., 2016; Shi et al., 2015). Metabolic realignment as a consequence of

203 interference with lipid homeostasis, which results in enhanced glycolysis may contribute to *Mtb*
204 growth restriction in these mutant macrophages.
205
206 **Knockout of lipid import and metabolism genes in macrophages activates AMPK and stabilizes**
207 **HIF1α**
208 *Mtb* infection is known to induce increased glycolysis or the "Warburg effect" in macrophages,
209 mouse lungs and human TB granulomas (Shi et al., 2015; Gleeson et al., 2016; Belton et al.,
210 2016). Several studies have demonstrated that the Warburg effect is mediated by the master
211 transcription factor hypoxia-inducible factor 1 (HIF1) (Courtnay et al., 2015). During *Mtb*
212 infection, HIF1 is activated by production of reactive oxygen species (ROS), TCA cycle
213 intermediates and hypoxia in the cellular microenvironments as a consequence of altered
214 metabolic activities and increased immune cell functions (Li et al., 2024; Shi et al., 2015;
215 Gleeson et al., 2016; Belton et al., 2016). We assessed HIF1 stability in the three mutant
216 macrophage lineages (FATP1$^{-/-}$, PLIN2$^{-/-}$ and CPT2$^{-/-}$) by monitoring total HIF1α protein levels by
217 western blot, having confirmed that they were all more glycolytically active than the scrambled
218 controls (Figure 2, Figure 2 - figure supplement 1). Indeed, all the three mutant macrophages
219 displayed significantly higher amounts of total HIF1α when compared to scrambled controls
220 after *Mtb* infection for 48 hours (Figure 3A, 3B, Figure 3 - figure supplement 1A, 1B). FATP1$^{-/-}$,
221 PLIN2$^{-/-}$ macrophages had increased levels of total HIF1α even in uninfected states (Figure 3A,
222 3B, Figure 3 - figure supplement 1A, 1B). We also checked the phosphorylation status of the
223 adenosine monophosphate kinase (AMPK), a master regulator of cell energy homeostasis
224 (Garcia and Shaw, 2017), in the mutant macrophages since Seahorse flux analyses indicated that
225 they had impaired mitochondrial activities (Figure 2, Figure 2 - figure supplement 1). Western
226 blot analysis revealed that in both *Mtb* infected and uninfected conditions, impaired fatty acid
227 metabolism in the mutant macrophages correlated with increased activation of AMPK as
228 indicated by higher levels of phosphorylated AMPK when compared to scramble (Figure 3C, 3D,
229 Figure 3 - figure supplement 1C, 1D). Interestingly, total AMPK was also increased, at least in
230 FATP1$^{-/-}$ and PLIN2$^{-/-}$ macrophages, in both uninfected and *Mtb* infected conditions (Figure 3C,
231 3E, Figure 3 - figure supplement 1C, 1D). These data point to a metabolic reprogramming of cells

232 through activation of HIF1α and AMPK to promote glycolysis. In energetically stressed cellular
233 environments, activated AMPK promotes catabolic processes such as autophagy to maintain
234 nutrient supply and energy homeostasis (Garcia and Shaw, 2017). Autophagy is also an innate
235 immune defense mechanism against intracellular *Mtb* in macrophages (Gutierrez et al., 2004).
236 We examined the levels of autophagic flux in the mutant macrophages by monitoring LC3I to
237 LC3II conversion by western blot and by qPCR analysis of selected autophagy genes (*AMBRA1*,
238 *ATG7*, *MAP1LC3B* and *ULK1)*. We observed an increase in autophagic flux by western blot
239 analysis of LC3II/LC3I ratios in *Mtb* infected FATP1$^{-/-}$ and CPT2$^{-/-}$ macrophages (Figure 3 - figure
240 supplement 2A-C). CPT2$^{-/-}$ macrophages were more autophagic even in uninfected conditions
241 (Figure 3 - figure supplement 2A-C). Meanwhile, our qPCR analysis also revealed that the four
242 autophagy genes were upregulated in both *Mtb* infected and uninfected conditions in all the
243 three mutants (Figure 3 - figure supplement 2D, 2E). These data suggest that impaired fatty acid
244 import and metabolism in macrophages could be restricting *Mtb* growth by promoting
245 autophagy. These data agree with previous observations that inhibition of fatty acid oxidation
246 enhances macrophage xenophagic activity which leads to improved control of *Mtb* (Chandra et
247 al., 2020).
248
249 **Exogenous oleate fails to rescue the *Mtb icl1*-deficient mutant in FATP1$^{-/-}$, PLIN2$^{-/-}$ and CPT2$^{-/-}$**
250 **macrophages**
251 The mycobacterial isocitrate lyase (*icl1*) acts as an isocitrate lyase in the glyoxylate shunt and as
252 a methyl-isocitrate lyase in the methyl-citrate cycle (MCC) (Gould et al., 2006; McKinney et al.,
253 2000). *Mtb* uses the MCC to convert propionyl CoA originating from the breakdown of
254 cholesterol rings and β-oxidation of odd chain fatty acids into succinate and pyruvate, which are
255 eventually assimilated into the TCA cycle (Muñoz-Elías et al., 2006; Griffin et al., 2012). The
256 buildup of propionyl CoA is toxic to *Mtb* and the bacteria relies on the MCC together with the
257 incorporation of propionyl CoA to methyl-branched lipids in the cell wall as an internal
258 detoxification system (Muñoz-Elías et al., 2006; Savvi et al., 2008). *Mtb* propionyl CoA toxicity is,
259 in part, due to a cellular imbalance between propionyl CoA and acetyl CoA as an accumulation
260 of the former or paucity of the latter results in the propionyl CoA mediated inhibition of

261 pyruvate dehydrogenase (Lee et al., 2013). Consequently, *Mtb icl1* deficient mutants (*Mtb ⊿icl1*)
262 are unable to grow in media supplemented with cholesterol or propionate, or intracellularly in
263 macrophages (Lee et al., 2013). However, this growth inhibition could be rescued both in culture
264 and in macrophages by exogenous supply of acetate or even chain fatty acids which can be
265 oxidized to acetyl-CoA (Lee et al., 2013). We took advantage of this metabolic knowledge to
266 assess whether exogenous addition of the even chain fatty acid oleate can rescue the
267 intracellular growth of *Mtb ⊿icl1* mutants in our CRISPR knockout macrophages. Scrambled
268 controls, FATP1$^{-/-}$, PLIN2$^{-/-}$ and CPT2$^{-/-}$ macrophages in normal macrophage media or media
269 supplemented with oleate were infected with an *Mtb ⊿icl1* strain expressing mCherry at MOI 5.
270 Bacterial growth measured by mCherry expression was recorded 5 days post infection.
271 Consistent with previous observations (Lee et al., 2013), the *Mtb ⊿icl1* mutant failed to replicate
272 in both mutant and scramble macrophages that were grown in normal macrophage media as
273 evidenced by baseline mCherry fluorescence (Figure 4A). Oleate supplementation successfully
274 rescued the *Mtb ⊿icl1* mutant in scrambled control macrophages. However, the growth
275 restriction of the *Mtb ⊿icl1* strain could not be alleviated by exogenous addition of oleate to the
276 mutant macrophages (FATP1$^{-/-}$, PLIN2$^{-/-}$ and CPT2$^{-/-}$) (Figure 4A). These data suggest that
277 impaired import (FATP1$^{-/-}$), sequestration (PLIN2$^{-/-}$) or β-oxidation of fatty acids (CPT2$^{-/-}$) blocks
278 *Mtb*'s ability to access and use cellular lipids.

279 Oleate supplementation in macrophages induces the formation of lipid droplets and we
280 were able to confirm the inability to produce lipid droplets in PLIN2$^{-/-}$ macrophages using this
281 approach (Figure 1 - figure supplement 2A). As an indirect measure to track the fate of
282 supplemented oleate in the mutant macrophages, we monitored lipid droplet biogenesis in
283 FATP1$^{-/-}$ and CPT2$^{-/-}$ macrophages to check if the inability to rescue the *Mtb ⊿icl1* impaired
284 growth phenotypes in these mutant macrophages could be possibly related to disruptions in
285 lipid droplet formation. Confocal analysis of BODIPY stained cells upon oleate supplementation
286 revealed that FATP1$^{-/-}$ macrophages also fail to generate lipid droplets (Figure 4B). In contrast,
287 CPT2$^{-/-}$ macrophages produced more and larger lipid droplets in comparison to scrambled
288 controls (Figure 4B). These data suggest that the inhibition of *Mtb* growth in these mutant
289 macrophages is not merely through limitation of access to fatty acid nutrients.

290
291
292
293
294 **Dual RNA sequencing to identify host and bacterial determinants of *Mtb* restriction in mutant**
295 **macrophage lineages.**
296 We performed RNA sequencing of both host and bacteria in *Mtb* infected mutant macrophages
297 as a preliminary step in identification of pathways restricting bacterial growth. We infected
298 scrambled controls, FATP1$^{-/-}$, PLIN2$^{-/-}$ and CPT2$^{-/-}$ macrophages with the *Mtb* smyc'::mCherry
299 strain for 4 days and processed the samples for dual RNA sequencing as previously described
300 (Simwela et al., 2024). Principal component analysis (PCA) of host transcriptomes revealed a
301 clustering of all the three mutant macrophages away from scrambled controls (Figure 5A).
302 Interestingly, there was a separation in transcriptional responses between the three mutant
303 macrophages as CPT2$^{-/-}$ and PLIN2$^{-/-}$ macrophages clustered closer together and more distant
304 from FATP1$^{-/-}$ (Figure 5A). Overall, using an adjusted p-value < 0.05 and absolute log2 fold
305 change > 1.2, we identified 900 genes which were differentially expressed (DE) in PLIN2$^{-/-}$
306 macrophages (589 up, 311 down), 817 genes which were DE in FATP1$^{-/-}$ macrophages (501 up,
307 315 down) and 189 genes which were DE in CPT2$^{-/-}$ (124 up, 65 down) (Supplementary file 2,
308 Figure 5B). Consistent with the PCA analysis, Venn diagram of the DE genes (Figure 5B) indicated
309 divergent responses in the three mutant macrophage populations. We performed pathway
310 enrichment analysis (Wu et al., 2021) of the DE genes to identify anti-microbial pathway
311 candidates in the three mutant macrophages. We found that defects in fatty acid uptake in
312 FATP1$^{-/-}$ infected macrophages upregulated pro-inflammatory pathways involved in MAPK and
313 ERK signaling and production of inflammatory cytokines (IFN-γ, interleukin-6, Interleukin-1α, β)
314 (Figure 6A, Supplementary file 3). The pro-inflammatory signatures of the FATP1$^{-/-}$ macrophages
315 are consistent with previous observations that demonstrated that a deficiency in FATP1
316 exacerbated macrophage activation *in vitro* and *in vivo* (Johnson et al., 2016). FATP1 is a solute
317 carrier family member (SLC27A1) and *Mtb* infected FATP1$^{-/-}$ macrophages showed reduced
318 expression of other solute carrier transporters (SLC) such as FATP4 (SLC27A4), GLUT1 (SLC2A1)

319 and 8 SLC amino acid transporters (Figure 6 - figure supplement 1A, 1B, 2A, Supplementary file
320 2). Interestingly, *Mtb* infected FATP1$^{-/-}$ macrophage transcriptomes exhibited upregulation of
321 macrophage scavenger receptors (MSR1) and the ATP binding cassette transporter ABCC1
322 (Figure 6 - figure supplement 1A), both of which can independently transport fatty acids into
323 cells (Vogel et al., 2022; Raggers et al., 1999).

324 Meanwhile, *Mtb* infection of PLIN2$^{-/-}$ macrophages led to upregulation in pathways
325 involved in ribosomal biology, MHC class 1 antigen presentation, canonical glycolysis, ATP
326 metabolic processes and type 1 interferon responses (Figure 6B, Supplementary file 3). In the
327 downregulated PLIN2$^{-/-}$ DE gene set, enriched pathways included those involved in production
328 of pro-inflammatory cytokines; interleukin-6 and 8, IFN-γ and interleukin-1 (Figure 6 - figure
329 supplement 2B, Supplementary file 3). Oxidative phosphorylation and processes involved in the
330 respiratory chain electron transport were also significantly enriched in PLIN2$^{-/-}$ downregulated
331 genes. This suggests that *Mtb* infected PLIN2$^{-/-}$ macrophages increase glycolytic flux and
332 decrease mitochondrial activities, which is consistent with our metabolic flux analysis data
333 (Figure 2, Figure 2 - figure supplement 1). Unlike FATP1$^{-/-}$ macrophages, PLIN2$^{-/-}$ macrophages
334 are, however, broadly anti-inflammatory as most pro-inflammatory genes were downregulated
335 upon *Mtb* infection.

336 Further downstream in the lipid processing steps, inhibition of fatty acid oxidation in
337 CPT2$^{-/-}$ macrophages upregulated pathways involved in MHC class 1 antigen presentation,
338 response to IFN-γ and interleukin-1 and T-cell mediated immunity (Figure 6 - figure supplement
339 3, Supplementary file 3). There was a limited overlap in enriched pathways in the upregulated
340 genes between *Mtb* infected CPT2$^{-/-}$ and FATP1$^{-/-}$ macrophages such as those involved in the
341 cellular responses to interleukin-1 and IFN-γ. However, many pathways over-represented in
342 CPT2$^{-/-}$ macrophages were common to PLIN2$^{-/-}$ macrophages (Figure 6B, Figure 6 - figure
343 supplement 3, Supplementary file 3). Similarly, both *Mtb*-infected PLIN2$^{-/-}$ *and* CPT2$^{-/-}$
344 macrophages were downregulated in expression of genes involved in oxidative phosphorylation
345 (Supplementary file 3). We confirmed expression levels of a selected genes by qPCR analysis of
346 IL-1β and the type 1 interferon (IFN-β) response during the early time points of infection.
347 Indeed, 4 hours post infection, IL-1β and IFN-β were both upregulated in FATP1$^{-/-}$ macrophages

348 as compared to scrambled controls consistent with their pro-inflammatory phenotype (Figure 6
349 - figure supplement 4A, 4B). On the contrary, PLIN2$^{-/-}$ macrophages downregulated IL-1β (Figure
350 6 - figure supplement 4B). These data indicate that macrophages respond quite divergently to
351 the deletion of the different steps in fatty acid uptake, which implies that the intracellular
352 pressures to which *Mtb* is exposed may also differ.
353
354 **Oxidative stress and nutrient limitation are major stresses experienced by *Mtb* in PLIN2$^{-/-}$ and**
355 **CPT2$^{-/-}$ macrophages**
356 We also analyzed transcriptomes from intracellular *Mtb* from scrambled controls, FATP1$^{-/-}$, CPT2^{-}
357 $^{/-}$ and PLIN2$^{-/-}$ macrophages in parallel with host transcriptomes in Figure 5A. Using an adjusted
358 p-value of < 0.1 and an absolute log2 fold change > 1.4, 0 genes were DE in FATP1$^{-/-}$
359 macrophages, 105 *Mtb* genes were DE in PLIN2$^{-/-}$ macrophages (69 up, 36 down) and 10 genes
360 were DE in CPT2$^{-/-}$ macrophages (3 up, 7 down) (Supplementary file 4). Despite being restrictive
361 to *Mtb* growth (Figure 1B) and appearing more pro-inflammatory (Figure 6A), FATP1$^{-/-}$
362 macrophages did not elicit a detectable shift in the transcriptional response in *Mtb,* compared
363 to control host cells. We speculate that pro-inflammatory responses in FATP1$^{-/-}$ macrophages
364 could be enough to restrict the growth of bacteria, but the resulting compensatory responses as
365 evidenced by the upregulation of macrophage scavenger receptors (Figure 6 - figure
366 supplement 1A) alleviate some of the stresses that a lack of fatty acid import could be duly
367 exerting on the bacteria. PLIN2$^{-/-}$ macrophages appeared to elicit the strongest transcriptional
368 response from *Mtb* which is consistent with our CFU data (Figure 1B) as PLIN2$^{-/-}$ macrophages
369 exhibited the strongest growth restriction. Among the DE genes in *Mtb* from PLIN2$^{-/-}$
370 macrophages (Supplementary file 4), a significant number of upregulated genes are involved in
371 nutrient assimilation (Figure 7A). *Mtb* in PLIN2$^{-/-}$ macrophages upregulated CobU (Rv0254c)
372 which is predicted to be involved in the bacteria's cobalamin (Vitamin B_{12}) biosynthesis. Vitamin
373 B_{12} is an important cofactor for the activity of *Mtb* genes required for cholesterol and fatty acid
374 utilization (Campos-Pardos et al., 2024; Savvi et al., 2008). Genes involved in de novo long chain
375 fatty acid synthesis (AccE5, Rv281) (Bazet Lyonnet et al., 2014), cholesterol breakdown (HsaD,
376 Rv3569c) (Lack et al., 2010), β-oxidation of fatty acids (EchA18, Rv3373; FadE22, Rv3061c)

377 (Schnappinger et al., 2003), purine salvage (Apt, Rv2584c) (Warner et al., 2014) and tryptophan
378 metabolism (Lott, 2020) were also upregulated in *Mtb* from PLIN2$^{-/-}$ macrophages (Figure 7A).
379 This metabolic re-alignment response is seen most frequently under nutrient limiting conditions
380 (Huang et al., 2018; Pisu et al., 2020; Theriault et al., 2022). *Mtb* in PLIN2$^{-/-}$ macrophages also
381 appears to experience a significant level of other cellular stresses as genes involved in DNA
382 synthesis and repair, general response to oxidative stress and PH survival in the phagosome
383 (DnaN, Rv0002; RecF, Rv0003; DinF, Rv2836c; Rv3242c, Rv1264) were upregulated (Figure 7B).
384 Amongst the down-regulated genes in *Mtb* in PLIN2$^{-/-}$ macrophages, FurA (Rv1909c), a KatG
385 repressor was the most significant (Figure 7B, Supplementary file 4). FurA downregulation
386 derepresses the catalase peroxidase, KatG, which promotes *Mtb* survival in oxidative stress
387 conditions (Zahrt et al., 2001). These data suggest that PLIN2$^{-/-}$ macrophages could be, in part,
388 restricting *Mtb* growth by increasing production of ROS. The data also suggest that, contrary to
389 a previous report (Knight et al., 2018), blocking lipid droplet formation in host macrophages
390 does place increased nutritional and oxidative stress on intracellular *Mtb*.
391 CPT2$^{-/-}$ macrophages elicited a modest shift in transcriptional response from *Mtb*, and
392 the majority of the DE genes (8 out of 10) were also DE in PLIN2$^{-/-}$ macrophages (Supplementary
393 file 4). This in in agreement with the host transcription response as CPT2$^{-/-}$ and PLIN2$^{-/-}$
394 macrophages share similar candidate anti-bacterial responses (Figure 5A, 5B, Figure 6B, Figure 6
395 - figure supplement 3). In common with the *Mtb* transcriptome response in PLIN2$^{-/-}$
396 macrophages, upregulated genes in *Mtb* isolated from CPT2$^{-/-}$ macrophages included those
397 involved in response to oxidative stress (DinF, Rv2836c) (Figure 7B, Supplementary file 4). To
398 substantiate some of these pathways, we assessed the levels of total cellular ROS in FATP1$^{-/-}$,
399 PLIN2$^{-/-}$ and CPT2$^{-/-}$ macrophages in both *Mtb* infected and uninfected conditions by staining the
400 cells with the Invitrogen CellROX dye and confocal microscopy analysis of live stained cells. In
401 both infected and uninfected conditions, all the three mutants displayed significantly elevated
402 total cellular ROS when compared to scramble controls (Fig. 7 - figure supplement 1A, 1B).
403
404 **Inhibitors of lipid metabolism block intracellular growth of *Mtb* in macrophages but not in**
405 **broth culture**

406 We next examined if pharmacological inhibitors would phenocopy the growth inhibition
407 phenotypes we observed with specific gene deletions. Compounds which modulate lipid
408 homeostasis are currently being investigated for HDT against TB, which is an area of
409 considerable interest (Kim et al., 2020). Such compounds include metformin, a widely used anti-
410 diabetic drug which activates AMPK, inhibits fatty acid synthesis and promotes β-oxidation of
411 fatty acids (Fullerton et al., 2013; Singhal et al., 2014). Chemical inhibition of fatty acid β-
412 oxidation is already known to promote macrophage control of *Mtb* (Chandra et al., 2020; Huang
413 et al., 2018). We targeted macrophage lipid homeostasis with trimetazidine (TMZ), an inhibitor
414 of β-oxidation of fatty acids, metformin, and an FATP1 inhibitor, FATP1 In (Matsufuji et al.,
415 2013). We assessed the impact of these compounds on extracellular *Mtb* cultured in broth over
416 9 days in the presence of the inhibitors (DMSO, TMZ; 500 nM, Metformin; 2 mM, FATP1 In; 10
417 μM, Rifampicin; 0.5 μg/ml). None of the three lipid metabolism inhibitors had a measurable
418 effect on *Mtb* growth in liquid culture media when compared to DMSO controls (Figure 8A).
419 Treatment with rifampicin completely blocked bacterial growth under the same conditions
420 (Figure 8A). We next infected scrambled sgRNA control macrophages with *Mtb* at MOI 0.5.
421 Inhibitors were added to infected macrophages 3 hours post infection and bacterial CFUs were
422 enumerated 4 days post treatment. Consistent with previous observations (Chandra et al., 2020;
423 Singhal et al., 2014), TMZ and metformin significantly reduced bacterial loads in macrophages
424 when compared to DMSO controls (Figure 8B). Similarly, FATP1 In also impacted the intracellular
425 growth of *Mtb* (Figure 8B). The results provide independent data that both genetic and
426 chemical modulation of fatty acid metabolism at different steps in the process negatively
427 impacts intracellular growth of *Mtb*.
428
429 **Discussion**
430 It is clearly established that host derived fatty acids and cholesterol are important carbon
431 sources for *Mtb* (Wilburn et al., 2018). However, the relationship between *Mtb* and the infected
432 host cell lipid metabolism remains a subject of conjecture. In this report, we characterized the
433 role of macrophage lipid metabolism on the intracellular growth of *Mtb* by a targeted CRISPR
434 mediated knockout of host genes involved in fatty acid import, sequestration and catabolism.

435 Macrophage fatty acid uptake is mediated by the scavenger receptor CD36 and specialized long
436 chain fatty acid transporters, FATP1 and FATP4 (Deng et al., 2023). Earlier studies reported that a
437 deficiency of CD36 enhances macrophage control of *Mtb,* albeit to a modest degree (Hawkes et
438 al., 2010). Work from Hawkes et al.(Hawkes et al., 2010) indicated that the anti-microbial
439 effectors in CD36 deficient macrophages were not due to bacterial uptake deficiencies,
440 differences in the rate of *Mtb* induced host cell death, production of ROS or pro-inflammatory
441 cytokines (Hawkes et al., 2010). We similarly observed a moderate *Mtb* growth restriction
442 phenotype in our CRISPR generated CD36$^{-/-}$ macrophages. However, a strong growth restriction
443 of *Mtb* was observed when we knocked out the long chain fatty acid transporter, FATP1. FATP1$^{-/-}$
444 macrophages displayed altered metabolism characterized by stabilization of HIF1α, activated
445 AMPK, increased glycolysis and reduced mitochondrial functions. Given that both CD36 and
446 FATP1 perform similar functions, it is expected that they should be some degree of
447 compensation between the transporters when either of the genes are deleted. Indeed, we
448 found out that FATP1 knockout resulted in the upregulation of other lipid import transporters
449 (MSR1, ABCC1). This would be consistent with the moderate anti-*Mtb* phenotypes in CD36$^{-/-}$
450 macrophages which could easily be compensated by the presence of FATPs to alleviate the
451 reduction in fatty acid supply experienced by intracellular *Mtb*. However, the FATP1$^{-/-}$
452 macrophage phenotype appears to be more severe on *Mtb* and could be exacerbated by an
453 elevated pro-inflammatory response as has been reported previously both *in vitro* and *in vivo*
454 (Johnson et al., 2016).
455
456 After uptake into the cells, most fatty acids either undergo β-oxidation in the mitochondria to
457 provide energy or are esterified with glycerol phosphate to form triacylglycerols that may be
458 incorporated into lipid droplets in the endoplasmic reticulum (Deng et al., 2023). Over the last 2
459 decades, it has been believed that lipid droplets are a nutrient source for *Mtb* in macrophages
460 (Russell et al., 2009; Daniel et al., 2011; Peyron et al., 2008; Singh et al., 2012). However, recent
461 work indicates lipid droplets may serve as centers for the production of pro-inflammatory
462 markers and anti-microbial peptides (Knight et al., 2018; Bosch et al., 2020). It has also been
463 reported that bone marrow macrophages derived from PLIN2$^{-/-}$ mice did not have defects in the

464 formation of lipid droplets and supported robust intracellular *Mtb* replication (Knight et al.,
465 2018). However, our mutant macrophages with myeloid specific knockout of PLIN2 are unable
466 to form lipid droplets and are defective in supporting the growth of *Mtb*. The discrepancies with
467 previous observations (Knight et al., 2018) could be a consequence of compensatory responses
468 to PLIN2 knockout in whole mice which when performed at embryonic level would allow for
469 sufficient time for the cells to recover by upregulating related PLIN isoforms. In fact, PLIN2$^{-/-}$
470 macrophages displayed the strongest anti-*Mtb* phenotypes amongst our mutants exhibiting
471 activated AMPK, increased glycolysis and autophagy and impaired mitochondrial functions. *Mtb*
472 isolated from PLIN2$^{-/-}$ macrophages displayed signatures of severe nutrient limitation and
473 oxidative stress damage.

474 It has also been previously reported that chemical, genetic or miR33 mediated blockade
475 of fatty acid β-oxidation in macrophages induces lipid droplet formation (Chandra et al., 2020;
476 Ouimet et al., 2016) but that this enhanced lipid droplet formation does not correlate with
477 improved intracellular *Mtb* growth (Chandra et al., 2020). We observed a similar phenotype as
478 CPT2$^{-/-}$ macrophages that generated larger and more abundant lipid droplets than scrambled
479 control macrophages were still restrictive to *Mtb* growth. This implies that the presence or
480 absence of lipid droplets does not in itself indicate whether a macrophage will support or
481 restrict *Mtb* growth, and that the anti-microbial environment extends beyond simple nutrient
482 availability.

483

484 In summary, our study shows that blocking macrophage's ability to import, sequester or
485 catabolize fatty acids chemically or by genetic knockout impairs *Mtb* intracellular growth. There
486 are shared features between potential anti-microbial effectors in macrophages which lack the
487 ability to import (FATP1$^{-/-}$) or metabolize fatty acids (PLIN2$^{-/-}$, CPT2$^{-/-}$) such as increased
488 glycolysis, stabilized HIF1α, activated AMPK, enhanced autophagy and production of ROS.
489 However, there are also intriguing points of divergence as FATP1$^{-/-}$ macrophages are more pro-
490 inflammatory while PLIN2$^{-/-}$ macrophages appear to be broadly anti-inflammatory. The routes
491 to *Mtb* growth restriction in these mutant macrophages are clearly more complex than the
492 bacteria's inability to acquire nutrients. The data further emphasizes that targeting fatty acid

493 homeostasis in macrophages at different steps in the process (uptake, storage and catabolism) is
494 worthy of exploring in the development of new therapeutics against tuberculosis.
495
496
497
498
499 **Materials and methods**
500 All materials and methods are as described (Simwela et al., 2024) unless otherwise specified.
501
502 **Flow cytometry and western blot analysis**
503 Generation of CRISPR mutant Hoxb8 macrophages was carried out as described previously
504 (Simwela et al., 2024). Antibodies used for both western blot and flow cytometry were as
505 follows: rat anti-Mouse CD36:Alexa Fluor®647 (Biorad, 10 µl/million cells), rabbit anti-PLIN2
506 (Proteintech, 1:1000), rabbit anti-FATP1 (Affinity biosciences, 1:1000), rabbit anti-CPT1A
507 antibody (Proteintech, 1:1000), rabbit anti-CPT2 antibody (Proteintech, 1:1000), rabbit anti-
508 HIF1α antibody (Proteintech, 1:1000), rabbit anti-AMPKα(1:1000, Cell signalling Technology),
509 rabbit anti-Phospho-AMPKα(1:500, Cell signalling Technology), rabbit anti-LC3B (1:1000, Cell
510 signalling Technology) and rabbit anti-β Actin (1:1000, Cell Signalling Technology). For western
511 blots, secondary antibodies used were anti-rabbit/mouse StarBright Blue 700 (1:2500, Biorad).
512 Blots were developed and imaged as described previously (Simwela et al., 2024).
513
514 **Staining for cellular lipid droplets**
515 Macrophages monolayers in Ibidi eight-well chambers were supplemented with exogenous 400
516 µM oleate for 24 hours to induce the formation of lipid droplets (Listenberger and Brown,
517 2007). Cells were then fixed in 4% paraformaldehyde and stained with BODIPY™ 493/503
518 (Invitrogen, 1 µg/ml) in 150 mM sodium chloride. Stained cells were mounted with media
519 containing DAPI and imaged using a Leica SP5 confocal microscope.
520
521 **Seahorse XF palmitate oxidation stress test**

522 A modified Seahorse mitochondrial stress test was used to measure macrophage's ability to
523 oxidize palmitate in substrate limiting conditions. Two days before the assay, 1 x 10^5 cells were
524 plated in Seahorse cell culture mini plates. One day before the assay, macrophage media was
525 replaced with the Seahorse substrate limited growth media (DMEM without pyruvate
526 supplemented with 0.5 mM glucose, 1 mM glutamine, 1% FBS and 0.5 mM L-Carnitine). On the
527 day of the assay, substrate limited media was replaced with assay media (DMEM without
528 pyruvate supplemented with 2 mM glucose and 0.5 mM L-Carnitine). In selected treatment
529 conditions, cells were either supplied with bovine serum albumin (BSA), BSA palmitate or BSA
530 palmitate plus etomoxir (4 µM). Oxygen consumption rates (OCRs) were measured using the
531 Mito Stress Test assay conditions as described previously (Simwela et al., 2024).
532
533 **Rescue of the *Mtb* ΔicI1 mutant in oleate supplemented media**
534 The *Mtb* H37Rv Δ*icl1* mutant expressing mCherry (Lee et al., 2013) was used for the rescue
535 experiments. The strain was maintained in 7H9 OADC broth as previously described (Simwela et
536 al., 2024) in the presence of Kanamycin (25 µg/ml) and hygromycin (50 µg/ml). 24 hours before
537 infection, macrophages were cultured in normal macrophage media or media supplemented
538 with 400 µM oleate. Cells were then infected with the *Mtb* Δ*icl1* mutant at MOI 5. The bacterial
539 mCherry signal was measured on day 0 and day 5 post infection on an Envision plate reader
540 (PerkinElmer). Oleate was maintained throughout the experiment in the rescue assay
541 conditions.
542
543 **Measurement of total cellular ROS**
544 Uninfected or *Mtb* infected macrophages monolayers in Ibidi eight-well chambers were stained
545 with the CellROX Deep Red dye (Invitrogen) as per manufacturer's staining protocol. Live stained
546 cells were imaged on a Leica SP5 confocal microscope. Z-stacks were re-constructed in ImageJ
547 from which mean fluorescence intensities (MFI) for individual cells were obtained.
548
549 **Datasets**

550 The RNA-seq data from the dual RNA-seq analysis of infected mouse macrophages, which
551 includes both macrophage and *Mtb* reads are available in GEO: GSE270571.
552 https://www.ncbi.nlm.nih.gov/geo/query/acc.cgi?acc=GSE270571
553

554 **Acknowledgements**

555 We would like to thank Dr. Jen K. Grenier and Ann E. Tate from the Cornell BRC Transcriptional
556 Regulation and Expression Facility for their help with the development of dual RNA-Seq
557 protocols. This work was supported by grants from the National Institutes of Health (AI155319,
558 AI162598, and OD032135), Bill and Melinda Gates Foundation and the Mueller Health
559 Foundation to D.G.R. EJ was supported by T32AI007349.
560

561 **References**
562

563 Almeida, P. E., Silva, A. R., Maya-Monteiro, C. M., Töröcsik, D., D'avila, H., Dezsö, B., et al. 2009.
564 *Mycobacterium bovis bacillus Calmette-Guérin* infection induces TLR2-dependent peroxisome
565 proliferator-activated receptor gamma expression and activation: functions in inflammation,
566 lipid metabolism, and pathogenesis. J Immunol, **183,** 1337-1345.

567 Bazet Lyonnet, B., Diacovich, L., Cabruja, M., Bardou, F., Quémard, A., Gago, G. & Gramajo, H.
568 2014. Pleiotropic effect of AccD5 and AccE5 depletion in acyl-coenzyme A carboxylase activity
569 and in lipid biosynthesis in *Mycobacteria*. PLoS One, **9,** e99853.

570 Belton, M., Brilha, S., Manavaki, R., Mauri, F., Nijran, K., Hong, Y. T., et al. 2016. Hypoxia and
571 tissue destruction in pulmonary TB. Thorax, **71,** 1145-1153.

572 Bosch, M., Sánchez-Álvarez, M., Fajardo, A., Kapetanovic, R., Steiner, B., Dutra, F., et al. 2020.
573 Mammalian lipid droplets are innate immune hubs integrating cell metabolism and host
574 defense. Science, **370**, eaay8085.

575 Brzostek, A., Pawelczyk, J., Rumijowska-Galewicz, A., Dziadek, B. & Dziadek, J. 2009.
576 *Mycobacterium tuberculosis* is able to accumulate and utilize cholesterol. J Bacteriol, **191,** 6584-
577 6591.

578 Campos-Pardos, E., Uranga, S., Picó, A., Gómez, A. B. & Gonzalo-Asensio, J. 2024. Dependency
579 on host vitamin B12 has shaped *Mycobacterium tuberculosis* complex evolution. Nat Commun,
580 **15,** 2161.

581 Chandra, P., He, L., Zimmerman, M., Yang, G., Köster, S., Ouimet, M., et al. 2020. Inhibition of
582 fatty acid oxidation promotes macrophage control of *Mycobacterium tuberculosis.* mBio, **11**,
583 e01139-20

584 Cohen, S. B., Gern, B. H., Delahaye, J. L., Adams, K. N., Plumlee, C. R., Winkler, J. K., et al. 2018.
585 Alveolar macrophages provide an early *Mycobacterium tuberculosis* niche and initiate
586 dissemination. Cell Host Microbe, **24,** 439-446.e4.

587 Conant, D., Hsiau, T., Rossi, N., Oki, J., Maures, T., Waite, K., et al. 2022. Inference of CRISPR Edits
588 from Sanger trace data. CRISPR J, **5,** 123-130.

589 Courtnay, R., Ngo, D. C., Malik, N., Ververis, K., Tortorella, S. M. & Karagiannis, T. C. 2015. Cancer
590 metabolism and the Warburg effect: the role of HIF-1 and PI3K. Mol Biol Rep, **42,** 841-851.

591 Cumming, B. M., Addicott, K. W., Adamson, J. H. & Steyn, A. J. 2018. *Mycobacterium*
592 *tuberculosis* induces decelerated bioenergetic metabolism in human macrophages. Elife, **7**,
593 e39169.

594 Daniel, J., Maamar, H., Deb, C., Sirakova, T. D. & Kolattukudy, P. E. 2011. *Mycobacterium*
595 *tuberculosis* uses host triacylglycerol to accumulate lipid droplets and acquires a dormancy-like
596 phenotype in lipid-loaded macrophages. PLoS Pathog, **7,** e1002093.

597 Deng, L., Kersten, S. & Stienstra, R. 2023. Triacylglycerol uptake and handling by macrophages:
598 from fatty acids to lipoproteins. Prog Lipid Res, **92,** 101250.

599 Fullerton, M. D., Galic, S., Marcinko, K., Sikkema, S., Pulinilkunnil, T., Chen, Z. P., et al. 2013.
600 Single phosphorylation sites in Acc1 and Acc2 regulate lipid homeostasis and the insulin-
601 sensitizing effects of metformin. Nat Med, **19,** 1649-1654.

602 Garcia, D. & Shaw, R. J. 2017. AMPK: Mechanisms of cellular energy sensing and restoration of
603 metabolic balance. Mol Cell, **66,** 789-800.

604 Gleeson, L. E., Sheedy, F. J., Palsson-Mcdermott, E. M., Triglia, D., O'leary, S. M., O'sullivan, M. P.,
605 et al. 2016. Cutting edge: *Mycobacterium tuberculosis* induces aerobic glycolysis in human
606 alveolar macrophages that is required for control of intracellular bacillary replication. J
607 Immunol, **196,** 2444-2449.

608 Gould, T. A., Van De Langemheen, H., Muñoz-Elías, E. J., Mckinney, J. D. & Sacchettini, J. C. 2006.
609 Dual role of isocitrate lyase 1 in the glyoxylate and methylcitrate cycles in *Mycobacterium*
610 *tuberculosis.* Mol Microbiol, **61,** 940-947.

611 Griffin, J. E., Pandey, A. K., Gilmore, S. A., Mizrahi, V., Mckinney, J. D., Bertozzi, C. R. & Sassetti, C.
612 M. 2012. Cholesterol catabolism by *Mycobacterium tuberculosis* requires transcriptional and
613 metabolic adaptations. Chem Biol, **19,** 218-227.

614 Gutierrez, M. G., Master, S. S., Singh, S. B., Taylor, G. A., Colombo, M. I. & Deretic, V. 2004.
615 Autophagy is a defense mechanism inhibiting BCG and *Mycobacterium tuberculosis* survival in
616 infected macrophages. Cell, **119,** 753-766.

617 Hawkes, M., Li, X., Crockett, M., Diassiti, A., Finney, C., Min-Oo, G., et al. 2010. CD36 deficiency
618 attenuates experimental *Mycobacterial* infection. BMC Infect Dis, **10,** 299.

619 Huang, L., Nazarova, E. V., Tan, S., Liu, Y. & Russell, D. G. 2018. Growth of *Mycobacterium*
620 *tuberculosis in vivo* segregates with host macrophage metabolism and ontogeny. J Exp Med,
621 **215,** 1135-1152.

622 Johnson, A. R., Qin, Y., Cozzo, A. J., Freemerman, A. J., Huang, M. J., Zhao, L., et al. 2016.
623 Metabolic reprogramming through fatty acid transport protein 1 (FATP1) regulates macrophage
624 inflammatory potential and adipose inflammation. Mol Metab, **5,** 506-526.

625 Kim, J. S., Kim, Y. R. & Yang, C. S. 2020. Host-directed therapy in tuberculosis: targeting host
626 metabolism. Front Immunol, **11,** 1790.

627 Kim, M. J., Wainwright, H. C., Locketz, M., Bekker, L. G., Walther, G. B., Dittrich, C., et al. 2010.
628 Caseation of human tuberculosis granulomas correlates with elevated host lipid metabolism.
629 EMBO Mol Med, **2,** 258-274.

630 Kim, Y. S., Lee, H. M., Kim, J. K., Yang, C. S., Kim, T. S., Jung, M., et al. 2017. PPAR-α activation
631 mediates innate host defense through induction of TFEB and lipid catabolism. J Immunol, **198,**
632 3283-3295.

633 Kiritsy, M. C., Mccann, K., Mott, D., Holland, S. M., Behar, S. M., Sassetti, C. M. & Olive, A. J.
634 2021. Mitochondrial respiration contributes to the interferon gamma response in antigen-
635 presenting cells. Elife, **10**, e65109

636 Knight, M., Braverman, J., Asfaha, K., Gronert, K. & Stanley, S. 2018. Lipid droplet formation in
637 *Mycobacterium tuberculosis* infected macrophages requires IFN-γ/HIF1α signaling and supports
638 host defense. PLoS Pathog, **14,** e1006874.

639 Lack, N. A., Yam, K. C., Lowe, E. D., Horsman, G. P., Owen, R. L., Sim, E. & Eltis, L. D. 2010.
640 Characterization of a carbon-carbon hydrolase from *Mycobacterium tuberculosis* involved in
641 cholesterol metabolism. J Biol Chem, **285,** 434-443.

642 Larigauderie, G., Furman, C., Jaye, M., Lasselin, C., Copin, C., Fruchart, J. C., et al. 2004.
643 Adipophilin enhances lipid accumulation and prevents lipid efflux from THP-1 macrophages:
644 potential role in atherogenesis. Arterioscler Thromb Vasc Biol, **24,** 504-510.

645 Lee, W., Vanderven, B. C., Fahey, R. J. & Russell, D. G. 2013. Intracellular *Mycobacterium*
646 *tuberculosis* exploits host-derived fatty acids to limit metabolic stress. J Biol Chem, **288,** 6788-
647 6800.

648 Li, C., Wang, J., Xu, J. F., Pi, J. & Zheng, B. 2024. Roles of HIF1α signaling in *Mycobacterium*
649 *tuberculosis* infection: new targets for anti-TB therapeutics? Biochem Biophys Res Commun,
650 **711,** 149920.

651 Listenberger, L. L. & Brown, D. A. 2007. Fluorescent detection of lipid droplets and associated
652 proteins. Curr Protoc Cell Biol, **Chapter 24,** Unit 24.2.

653 Lott, J. S. 2020. The tryptophan biosynthetic pathway is essential for *Mycobacterium*
654 *tuberculosis* to cause disease. Biochem Soc Trans, **48,** 2029-2037.

655 Matsufuji, T., Ikeda, M., Naito, A., Hirouchi, M., Kanda, S., Izumi, M., et al. 2013. Arylpiperazines
656 as fatty acid transport protein 1 (FATP1) inhibitors with improved potency and pharmacokinetic
657 properties. Bioorg Med Chem Lett, **23,** 2560-2565.

658 Mckinney, J. D., Höner Zu Bentrup, K., Muñoz-Elías, E. J., Miczak, A., Chen, B., Chan, W. T., et al.
659 2000. Persistence of *Mycobacterium tuberculosis* in macrophages and mice requires the
660 glyoxylate shunt enzyme isocitrate lyase. Nature, **406,** 735-738.

661 Muñoz-Elías, E. J. & Mckinney, J. D. 2005. *Mycobacterium tuberculosis* isocitrate lyases 1 and 2
662 are jointly required for *in vivo* growth and virulence. Nat Med, **11,** 638-644.

663 Muñoz-Elías, E. J., Upton, A. M., Cherian, J. & Mckinney, J. D. 2006. Role of the methylcitrate
664 cycle in *Mycobacterium tuberculosis* metabolism, intracellular growth, and virulence. Mol
665 Microbiol, **60,** 1109-1122.

666 Nishiyama, K., Fujita, T., Fujimoto, Y., Nakajima, H., Takeuchi, T. & Azuma, Y.-T. 2018. Fatty acid
667 transport protein 1 enhances the macrophage inflammatory response by coupling with
668 ceramide and c-Jun N-terminal kinase signaling. Int Immunopharmacol, **55,** 205-215.

669 Ouimet, M., Koster, S., Sakowski, E., Ramkhelawon, B., Van Solingen, C., Oldebeken, S., et al.
670 2016. *Mycobacterium tuberculosis* induces the miR-33 locus to reprogram autophagy and host
671 lipid metabolism. Nat Immunol, **17,** 677-686.

672 Pandey, A. K. & Sassetti, C. M. 2008. *Mycobacterial* persistence requires the utilization of host
673 cholesterol. Proc Natl Acad Sci U S A, **105,** 4376-4380.

674 Parihar, S. P., Guler, R., Khutlang, R., Lang, D. M., Hurdayal, R., Mhlanga, M. M., et al. 2014.
675 Statin therapy reduces the *Mycobacterium tuberculosis* burden in human macrophages and in
676 mice by enhancing autophagy and phagosome maturation. J Infect Dis, **209,** 754-763.

677 Paul, A., Chang, B. H., Li, L., Yechoor, V. K. & Chan, L. 2008. Deficiency of adipose differentiation-
678 related protein impairs foam cell formation and protects against atherosclerosis. Circ Res, **102,**
679 1492-501.

680 Peyron, P., Vaubourgeix, J., Poquet, Y., Levillain, F., Botanch, C., Bardou, F., et al. 2008. Foamy
681 macrophages from tuberculous patients' granulomas constitute a nutrient-rich reservoir for *M.*
682 *tuberculosis* persistence. PLoS Pathog, **4,** e1000204.

683 Pisu, D., Huang, L., Grenier, J. K. & Russell, D. G. 2020. Dual RNA-seq of Mtb-infected
684 macrophages *in vivo* reveals ontologically distinct host-pathogen interactions. Cell Rep, **30,** 335-
685 350 e4.

686 Pisu, D., Huang, L., Narang, V., Theriault, M., Le-Bury, G., Lee, B., et al. 2021. Single cell analysis
687 of *M. tuberculosis* phenotype and macrophage lineages in the infected lung. J Exp Med, **218**,
688 e20210615

689 Podinovskaia, M., Lee, W., Caldwell, S. & Russell, D. G. 2013. Infection of macrophages with
690 *Mycobacterium tuberculosis* induces global modifications to phagosomal function. Cell
691 Microbiol, **15,** 843-859.

692 Raggers, R. J., Van Helvoort, A., Evers, R. & Van Meer, G. 1999. The human multidrug resistance
693 protein MRP1 translocates sphingolipid analogs across the plasma membrane. J Cell Sci, **112 (Pt**
694 **3),** 415-422.

695 Russell, D. G., Cardona, P. J., Kim, M. J., Allain, S. & Altare, F. 2009. Foamy macrophages and the
696 progression of the human tuberculosis granuloma. Nat Immunol, **10,** 943-948.

697 Savvi, S., Warner, D. F., Kana, B. D., Mckinney, J. D., Mizrahi, V. & Dawes, S. S. 2008. Functional
698 characterization of a vitamin B12-dependent methylmalonyl pathway in *Mycobacterium*

699 *tuberculosis*: implications for propionate metabolism during growth on fatty acids. J Bacteriol,
700 **190,** 3886-3895.

701 Schnappinger, D., Ehrt, S., Voskuil, M. I., Liu, Y., Mangan, J. A., Monahan, I. M., et al. 2003.
702 Transcriptional adaptation of *Mycobacterium tuberculosis* within macrophages: insights into the
703 phagosomal environment. J Exp Med, **198,** 693-704.

704 Shi, L., Salamon, H., Eugenin, E. A., Pine, R., Cooper, A. & Gennaro, M. L. 2015. Infection with
705 *Mycobacterium tuberculosis* induces the Warburg effect in mouse lungs. Sci Rep, **5,** 18176.

706 Simwela, N. V., Johnston, L., Bitar, P. P., Jaecklein, E., Altier, C., Sassetti, C. M. & Russell, D. G.
707 2024. Genome-wide screen of *Mycobacterium tuberculosis*-infected macrophages revealed
708 GID/CTLH complex-mediated modulation of bacterial growth. Nat Commun, **15,** 9322.

709 Singh, V., Jamwal, S., Jain, R., Verma, P., Gokhale, R. & Rao, K. V. 2012. *Mycobacterium*
710 *tuberculosis*-driven targeted recalibration of macrophage lipid homeostasis promotes the foamy
711 phenotype. Cell Host Microbe, **12,** 669-681.

712 Singhal, A., Jie, L., Kumar, P., Hong, G. S., Leow, M. K., Paleja, B., et al. 2014. Metformin as
713 adjunct antituberculosis therapy. Sci Transl Med, **6,** 263ra159.

714 Theriault, M. E., Pisu, D., Wilburn, K. M., Lê-Bury, G., Macnamara, C. W., Michael Petrassi, H., et
715 al. 2022. Iron limitation in *M. tuberculosis* has broad impact on central carbon metabolism.
716 Commun Biol, **5,** 685.

717 Vogel, A., Brunner, J. S., Hajto, A., Sharif, O. & Schabbauer, G. 2022. Lipid scavenging
718 macrophages and inflammation. Biochim Biophys Acta Mol Cell Biol Lipids, **1867,** 159066.

719 Warner, D. F., Evans, J. C. & Mizrahi, V. 2014. Nucleotide metabolism and DNA replication.
720 Microbiol Spectr, **2**, MGM2-0001-2013.

721 WHO 2023. Global tuberculosis report 2023. Geneva, Switzerland World Health Organisation.

722 Wilburn, K. M., Fieweger, R. A. & Vanderven, B. C. 2018. Cholesterol and fatty acids grease the
723 wheels of Mycobacterium tuberculosis pathogenesis. Pathog Dis, **76**, fty021

724 Wolf, A. J., Linas, B., Trevejo-Nuñez, G. J., Kincaid, E., Tamura, T., Takatsu, K. & Ernst, J. D. 2007.
725 *Mycobacterium tuberculosis* infects dendritic cells with high frequency and impairs their
726 function *in vivo*. J Immunol, **179,** 2509-2519.

727 Wu, T., Hu, E., Xu, S., Chen, M., Guo, P., Dai, Z., et al. 2021. clusterProfiler 4.0: a universal
728 enrichment tool for interpreting omics data. Innovation (Camb), **2,** 100141.

729 Zahrt, T. C., Song, J., Siple, J. & Deretic, V. 2001. *Mycobacterial* FurA is a negative regulator of
730 catalase-peroxidase gene katG. Mol Microbiol, **39,** 1174-1185.
731
732
733 **Figure legends**
734 **Figure 1: Knockout of fatty acid import and metabolism genes restricts *Mtb* growth in**
735 **macrophages**. (A) Schematic of lipid import and metabolism genes in macrophages. Genes
736 targeted for CRISPR-Cas9 mediated knockout are highlighted in red. (B) Scramble or indicated
737 mutant macrophages were infected with the *Mtb* Erdman strain at MOI 0.4. Intracellular *Mtb*
738 growth was measured by plating and counting CFUs in lysed macrophages 5 days post infection
739 (PI). (C) CFUs from lysed macrophages were also plated on day 0, 3 hours post infection to
740 measure bacterial uptake differences. n=6 biological replicates; ****, $P < 0.0001$, one-way
741 ANOVA alongside Dunnett's multiple comparison test. Data are presented as mean
742 values±SD.
743
744 **Figure 2: *Mtb* infected macrophages with impaired fatty acid import and metabolism display**
745 **reduced mitochondrial activities and are more glycolytic**. (A) Seahorse flux analyses of
746 scramble or PLIN2$^{-/-}$, FATP1$^{-/-}$ and CPT2$^{-/-}$ macrophages infected with *Mtb* Erdman strain at MOI
747 1 24 hours post infection. Oxygen consumption rates (OCR) were measured using the Cell Mito
748 Stress Test Kit (Agilent). Oligo, oligomycin; FCCP, fluoro-carbonyl cyanide phenylhydrazone;
749 Rot/A, rotenone and antimycin A. (B) Comparison of basal respiration and spare respiratory

750 capacity (SRC) from A. SRC was calculated by subtracting the normalized maximal OCR from
751 basal OCR. n=3 biological replicates (2 technical repeats per replicate); ****, $P < 0.0001$, one-
752 way ANOVA alongside Dunnett's multiple comparison test. Data are presented as mean
753 values±SD. (C) Extracellular acidification rates (ECARs) of scramble or PLIN2$^{-/-}$, FATP1$^{-/-}$ and
754 CPT2$^{-/-}$ macrophages infected with *Mtb* as in A. ECARs were measured using the Agilent
755 Seahorse Glycolysis Stress Test kit. 2DG, 2-Deoxy-D-glucose. (D) Comparison of basal glycolysis
756 and spare glycolytic capacity (SGC) in the indicated mutant macrophages. SGC was calculated as
757 SRC above. n=3 biological replicates (2 technical repeats per replicate); *, $P < 0.05$, ****, $P <$
758 0.0001, one-way ANOVA alongside Dunnett's multiple comparison test. Data are presented as
759 mean values±SD.
760
761
762
763 **Figure 3: Knockout of fatty acid import and metabolism genes in macrophages activate AMPK**
764 **and stabilizes HIF1α.** (A) Western blot analysis of HIF1α in uninfected and *Mtb* infected
765 scramble or PLIN2$^{-/-}$, FATP1$^{-/-}$ and CPT2$^{-/-}$ macrophages. In *Mtb* infected conditions, cells were
766 infected with the bacteria at MOI 1 for 48 hours before preparation of cell lysates. (B)
767 Quantification of relative expression of HIF1α in (A) and in Figure 3 - figure supplements 1A, 1B
768 normalized to β-actin; n=3 biological replicates. *P<0.05; ***P<0.001, two-way ANOVA
769 alongside Dunnett's multiple comparison test. Data are presented as mean values±SD. (C)
770 Western blot analysis of total and phosphorylated AMPK in uninfected and *Mtb* infected
771 scramble or PLIN2$^{-/-}$, FATP1$^{-/-}$ and CPT2$^{-/-}$ *macrophages*. Cell lysates were prepared as in (A). (D,
772 E) Quantification of relative expression of pAMPK and AMPK in (C) and in Figure 3 - figure
773 supplements 1C, 1D normalized to β-actin; n=3 biological replicates. **P<0.01;
774 ***P<0.001, ****P<0.0001, two-way ANOVA alongside Dunnett's multiple comparison
775 test. Data are presented as mean values±SD.
776
777 **Figure 4: Supplementation with exogenous oleate fails to rescue the *Mtb* ΔicI1 mutant in**
778 **PLIN2$^{-/-}$, FATP1$^{-/-}$ and CPT2$^{-/-}$ macrophages**. (A) Scramble or indicated mutant macrophages

779 were infected with the *Mtb* H37Rv Δicl1 mutant expressing mCherry at MOI 5. Oleate
780 supplementation (400 μM) was commenced 24 hours before infection in the treatment group,
781 removed during *Mtb* infection and re-added 3-hours post infection for the entire duration of the
782 experiment. Growth kinetics of *Mtb* were measured by monitoring mCherry fluorescence using
783 a plate reader. n=4 biological replicates; ****, $P < 0.0001$, two-way ANOVA alongside Dunnett's
784 multiple comparison test. Data are presented as mean values ± SD. (B) Uninfected scramble or
785 FATP1$^{-/-}$ and CPT2$^{-/-}$ macrophages were supplemented with 400 μM oleate for 24 hours. Cells
786 were then fixed for 20 minutes and stained for lipid droplet inclusions using the Bodipy 493/503
787 dye. DAPI was used as a counterstain to detect nuclei.
788
789 **Figure 5: Dual RNA sequencing to identify host and bacterial determinants of *Mtb* restriction**
790 **in macrophages with fatty acid import and metabolism knockout genes**. (A) Principal
791 component analysis (PCA) of scramble or PLIN2$^{-/-}$, FATP1$^{-/-}$ and CPT2$^{-/-}$ macrophages
792 transcriptomes infected with the *Mtb* smyc'::mCherry strain at MOI 0.5 4 days post infection. (B)
793 Venn diagram of DE gene sets (Supplementary file 2) in PLIN2$^{-/-}$, FATP1$^{-/-}$ and CPT2$^{-/-}$ mutant
794 macrophages as compared to scramble showing overlapping genes. DE genes cutoff; abs ($\log_2$
795 fold change) > 0.3, adjusted p-value < 0.05.
796
797 **Figure 6: Pathway enrichment analysis of upregulated genes in *Mtb* infected PLIN2$^{-/-}$ and**
798 **FATP1$^{-/-}$ macrophages**
799 Tree plots of top 80 enriched gene ontology terms (biological process) in *Mtb* infected PLIN2$^{-/-}$
800 (A) and FATP1$^{-/-}$ (B) upregulated genes.
801
802 **Figure 7: Nutritional and oxidative stress define the core transcriptome response of *Mtb***
803 **inside PLIN2$^{-/-}$ macrophages**. Heatmaps of nutritional (A) and oxidative stress (B) DE genes in
804 PLIN2$^{-/-}$ macrophages. Arrows show genes which are also DE in CPT2$^{-/-}$ macrophages in a similar
805 trend (Supplementary file 4).
806

807 **Figure 8: Inhibitors of fatty acid transport and metabolism block intracellular growth of *Mtb* in**
808 **macrophages.** (A) Growth of *Mtb* in liquid broth in the absence of drug (DMSO) or presence of
809 metformin, FATP1 inhibitor (FATP1 In, 10 μM) and the β-oxidation of fatty acid inhibitor,
810 Trimetazidine (TMZ, 500 nM). *Mtb* Erdman was grown to log phase and diluted to OD_{600} 0.01 in
811 7H9 media in the presence of the above inhibitors. Growth kinetics were monitored by OD_{600}
812 measurements using a plate reader. Rifampicin (RIF) at 0.5 μg/ml was used as a total killing
813 control. (B) Scramble macrophages were infected with *Mtb* Erdman at MOI 0.5. Inhibitors were
814 added 3 hours post infection following which CFUs were plated 4 days post infection. n=5
815 biological replicates; **, $P < 0.01$; ****, $P < 0.0001$, one-way ANOVA alongside Dunnett's
816 multiple comparison test. Data are presented as mean values ± SD.
817
818
819
820
821
822 **Supplementary figure legends**
823 **Figure 1 - figure supplement 1: Flow cytometry and western blot analysis of CRISPR knockout**
824 **macrophages.** (A-E) Western blot and flow cytometry analysis of protein depletion in fatty acid
825 import and metabolism genes in macrophages derived from Hoxb8 parental lines
826 (Supplementary file 1). Each gene was targeted with at least 2 sgRNAs; PLIN2 (A), FATP1 (B),
827 CD36 (C), CPT1A (D), CPT2 (E).
828
829 **Figure 1 - figure supplement 2: Lipid droplet formation and fatty acid oxidation in PLIN2$^{-/-}$ and**
830 **CPT2$^{-/-}$ macrophages.** (A) Phenotypic characterization of lipid droplet biogenesis in PLIN2$^{-/-}$
831 macrophages. Uninfected macrophages were supplemented with 400 μM oleate for 24 hours.
832 Cells were fixed for 20 minutes and stained for lipid droplet inclusions using the Bodipy 493/503
833 dye. DAPI was used as a counterstain to detect nuclei. (B) Seahorse fatty acid oxidation analyses
834 of uninfected scramble or CPT2$^{-/-}$ macrophages. Cells were cultured in substrate limiting
835 conditions for 24 hours and supplied with exogenous palmitate. Oxygen consumption rates

836 (OCR) were measured as in the Cell Mito Stress Test Kit (Agilent). Oligo, oligomycin; FCCP, fluoro-
837 carbonyl cyanide phenylhydrazone; Rot/A, rotenone and antimycin A; BSA, bovine serum
838 albumin; Eto, Etomoxir. n=3 biological replicates; **, P < 0.01, one-way ANOVA alongside
839 Dunnett's multiple comparison test. Data are presented as mean values ± SD.
840
841 **Figure 2 - figure supplement 1: Flux analyzes of mitochondrial activities and glycolysis in**
842 **PLIN2$^{-/-}$, FATP1$^{-/-}$ and CPT2$^{-/-}$ macrophages.** (A) Seahorse flux analyses in uninfected scramble or
843 PLIN2$^{-/-}$, FATP1$^{-/-}$ and CPT2$^{-/-}$ macrophages using the Cell Mito Stress Kit as in Figure 2A, 2B. (B)
844 Seahorse flux analyses in uninfected scramble or PLIN2$^{-/-}$, FATP1$^{-/-}$ and CPT2$^{-/-}$ macrophages
845 using the Glycolysis Stress Test kit as in Figure 2C, 2D.
846
847 **Figure 3 - figure supplement 1:** Replicate western blot analyzes of HIF1α (A, B), AMPK and
848 pAMPK (C, D) in uninfected and *Mtb* infected scramble or PLIN2$^{-/-}$, FATP1$^{-/-}$ and CPT2$^{-/-}$
849 macrophages as in Figure 3.
850
851 **Figure 3 - figure supplement 2: Increased autophagy in PLIN2$^{-/-}$, FATP1$^{-/-}$ and CPT2$^{-/-}$**
852 **macrophages.** (A, B) Independent western blot analyzes of autophagic LC3I to LC3II conversion
853 in uninfected and *Mtb* infected scramble or PLIN2$^{-/-}$, FATP1$^{-/-}$ and CPT2$^{-/-}$ macrophages. (C)
854 Densitometry quantification of LC3I to LC3II turnover ratios (LC3II/LC3I ratio) in (A) and (B) after
855 normalization to β-actin; n = 2 biological replicates. *P < 0.05; **P < 0.01, two-way ANOVA
856 alongside Dunnett's multiple comparison test. Data are presented as mean values ± SD. (D, E)
857 qPCR analysis of the indicated autophagy genes in uninfected (D) and *Mtb* infected (E) scramble
858 or PLIN2$^{-/-}$, FATP1$^{-/-}$ and CPT2$^{-/-}$ macrophages. The *Mtb Erdman* strain was used for bacterial
859 infections. *, P < 0.05; **, P < 0.01; ***, P < 0.001; ****, P < 0.0001, two-way ANOVA alongside
860 Dunnett's multiple comparison test. Data are presented as mean values ± SD.
861
862 **Figure 6 - figure supplement 1. Compensatory transcriptional responses in *Mtb* infected**
863 **FATP1$^{-/-}$ macrophages.** (A, B) Violin plots showing expression (log2 normalized counts) of fatty
864 acid (A) and amino acid transport genes (B) in FATP1$^{-/-}$ mutant macrophages 4 days post

865 infection (Figure 5). *, P < 0.05; **, P < 0.01, ***, P < 0.001; ****, P < 0.0001, two-way ANOVA
866 alongside Dunnett's multiple comparison test. Data are presented as mean values ± SD.
867
868 **Figure 6 - figure supplement 2: Tree plot of top 80 enriched gene ontology terms (biological**
869 **process) in PLIN2$^{-/-}$ and FATP1$^{-/-}$ macrophages downregulated genes.**
870
871 **Figure 6 - figure supplement 3: Tree plot of top 80 enriched gene ontology terms (biological**
872 **process) in CPT2$^{-/-}$ macrophages upregulated genes.**
873
874 **Figure 6 - figure supplement 4: qPCR analysis of IFN-β and IL-1β in in PLIN2$^{-/-}$, FATP1$^{-/-}$ and**
875 **CPT2$^{-/-}$ macrophages.** Macrophages were left uninfected or infected with the *Mtb Erdman*
876 strain at MOI 4. RNA was extracted for qPCR at 4 and 24 hours post infection. ***, *P* < 0.001;
877 ****, *P* < 0.0001, two-way ANOVA alongside Dunnett's multiple comparison test. Data are
878 presented as mean values ± SD.
879
880 **Figure 7 - figure supplement 1: Total cellular ROS in PLIN2$^{-/-}$, FATP1$^{-/-}$ and CPT2$^{-/-}$ macrophages.**
881 (A-B) Scramble or PLIN2$^{-/-}$, FATP1$^{-/-}$ and CPT2$^{-/-}$ macrophages were left uninfected (A) or infected
882 (B) with the *Mtb* Erdman strain at MOI 1 for 24 hours. Live cells were stained with the Invitrogen
883 CellROX™ Deep Red dye and imaged using a confocal microscope. Mean fluorescence intensities
884 (MFI) per individual cell were quantified using ImageJ in at least 100 cells for every mutants
885 across three biological replicates. **, P < 0.01; ****, P < 0.0001, one-way ANOVA alongside
886 Dunnett's multiple comparison test. Data are presented as mean values ± SD.
887
888
889
890
891
892
893

894
895
896
897
898
899
900
901
902
903
904
905
906
907
908
909 **Description of supplementary files**
910 **Supplementary file 1**. sgRNAs Primers and ICE scores for lipid import and metabolism gene
911 targets in this study
912 **Supplementary file 2**. Differentially expressed genes in PLIN2$^{-/-}$, FATP1$^{-/-}$ and CPT2$^{-/-}$ *Mtb*
913 infected macrophages
914 **Supplementary file 3**. Enriched GO terms in upregulated and downregulated genes in PLIN2$^{-/-}$,
915 FATP1$^{-/-}$ and CPT2$^{-/-}$ *Mtb* infected macrophages
916 **Supplementary file 4**. *Mtb* differentially expressed genes in PLIN2$^{-/-}$ and CPT2$^{-/-}$ infected
917 macrophages
918
919
920
921
922

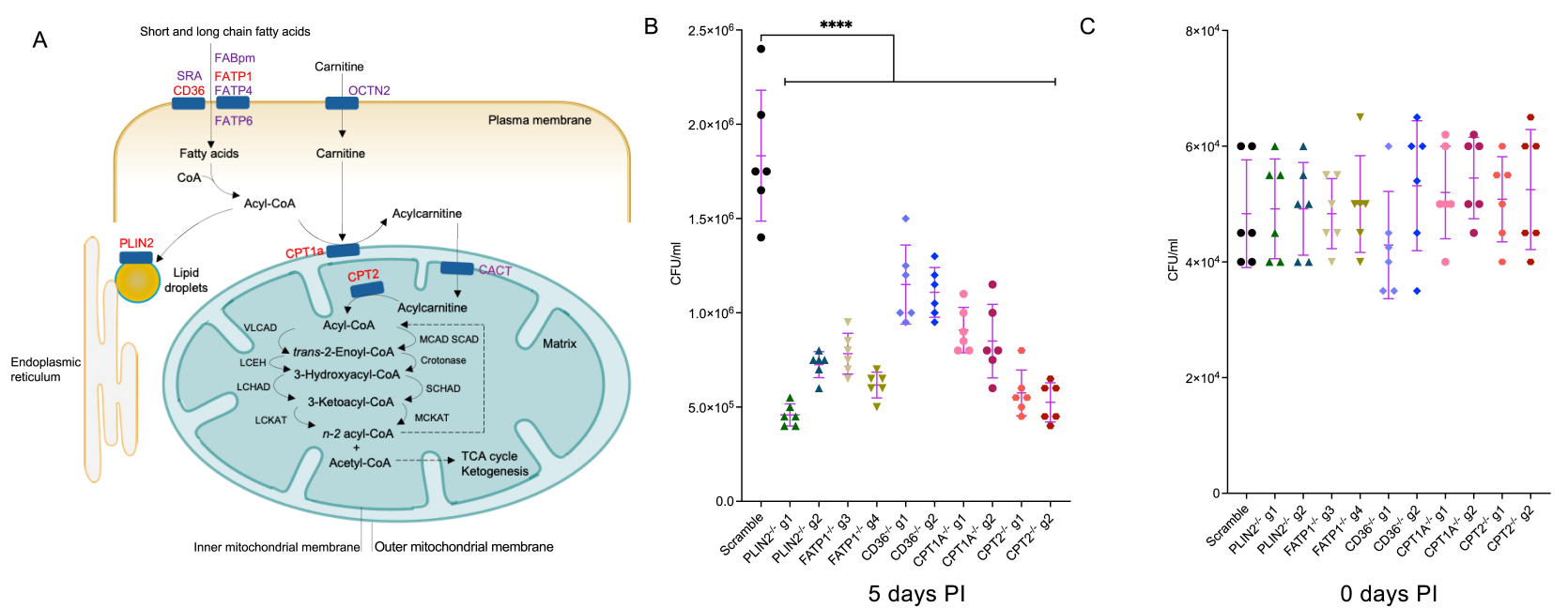
A
Short and long chain fatty acids
FABpm
SRA
CD36
FATP1
FATP4
FATP6
Carnitine
OCTN2
Plasma membrane
Fatty acids
Carnitine
CoA
Acyl-CoA
Acylcarnitine
PLIN2
Lipid droplets
CPT1a
CPT2
CACT
Acylcarnitine
Acyl-CoA
VLCAD
MCAD SCAD
trans-2-Enoyl-CoA
LCEH
Crotonase
3-Hydroxyacyl-CoA
LCHAD
SCHAD
3-Ketoacyl-CoA
LCKAT
MCKAT
n-2 acyl-CoA
+
Acetyl-CoA
TCA cycle
Ketogenesis
Matrix
Endoplasmic reticulum
Inner mitochondrial membrane
Outer mitochondrial membrane
B
****
CFU/ml
2.5×10^6
2.0×10^6
1.5×10^6
1.0×10^6
5.0×10^5
0.0
Scramble
PLIN2-/- g1
PLIN2-/- g2
FATP1-/- g3
FATP1-/- g4
CD36-/- g1
CD36-/- g2
CPT1A-/- g1
CPT1A-/- g2
CPT2-/- g1
CPT2-/- g2
5 days PI
C
CFU/ml
8×10^4
6×10^4
4×10^4
2×10^4
0
Scramble
PLIN2-/- g1
PLIN2-/- g2
FATP1-/- g3
FATP1-/- g4
CD36-/- g1
CD36-/- g2
CPT1A-/- g1
CPT1A-/- g2
CPT2-/- g1
CPT2-/- g2
0 days PI

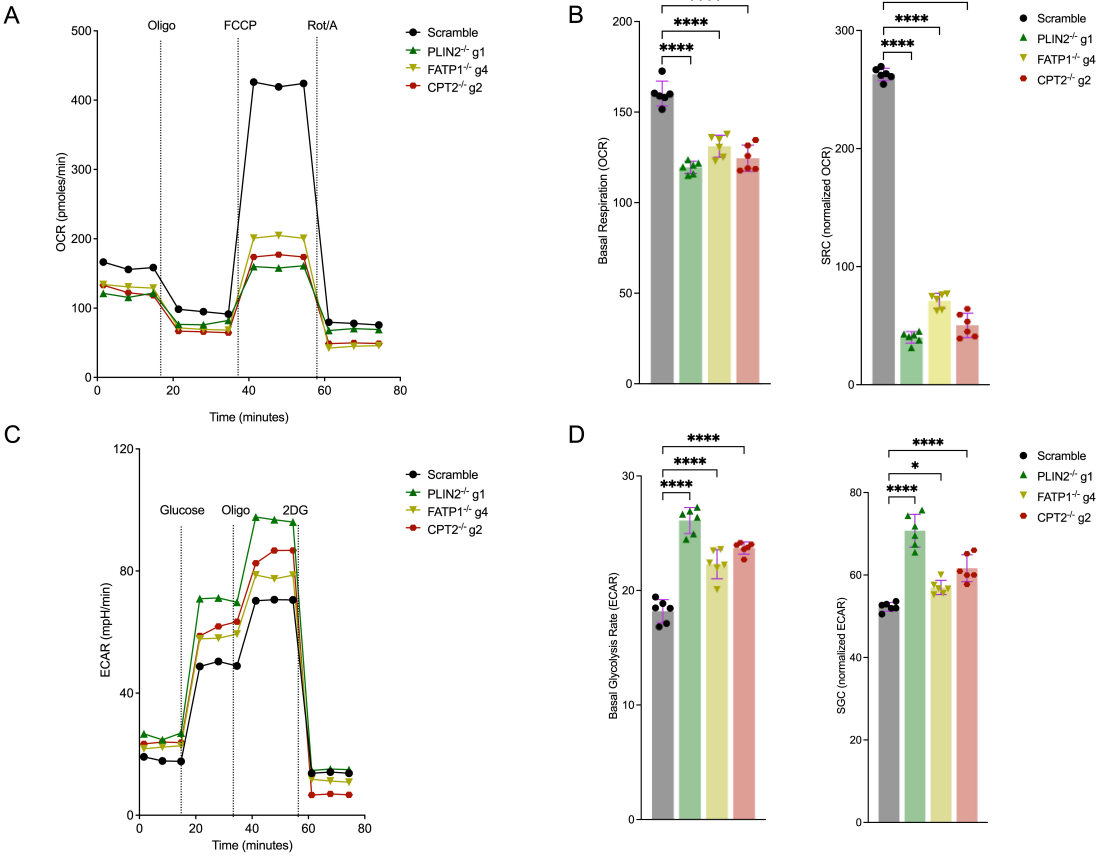
A
Oligo
FCCP
Rot/A
Scramble
PLIN2-/- g1
FATP1-/- g4
CPT2-/- g2
OCR (pmoles/min)
Time (minutes)
B
Basal Respiration (OCR)
SRC (normalized OCR)
****
C
Glucose
Oligo
2DG
ECAR (mpH/min)
Time (minutes)
D
Basal Glycolysis Rate (ECAR)
SGC (normalized ECAR)
*

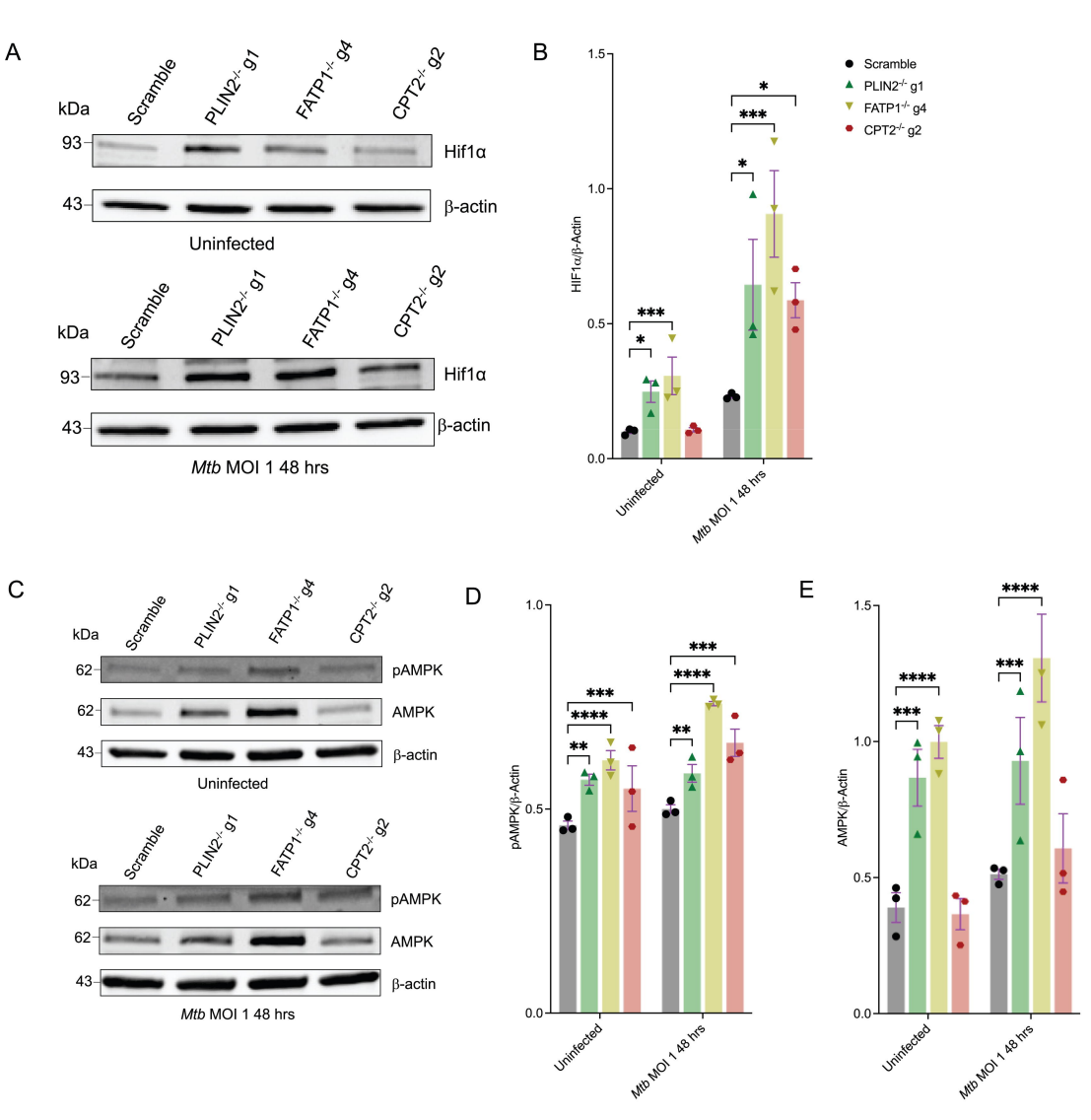
A
kDa
Scramble
PLIN2-/- g1
FATP1-/- g4
CPT2-/- g2
93
Hif1α
43
β-actin
Uninfected
Mtb MOI 1 48 hrs
B
HIF1α/β-Actin
Scramble
PLIN2-/- g1
FATP1-/- g4
CPT2-/- g2
C
62
pAMPK
AMPK
D
pAMPK/β-Actin
E
AMPK/β-Actin

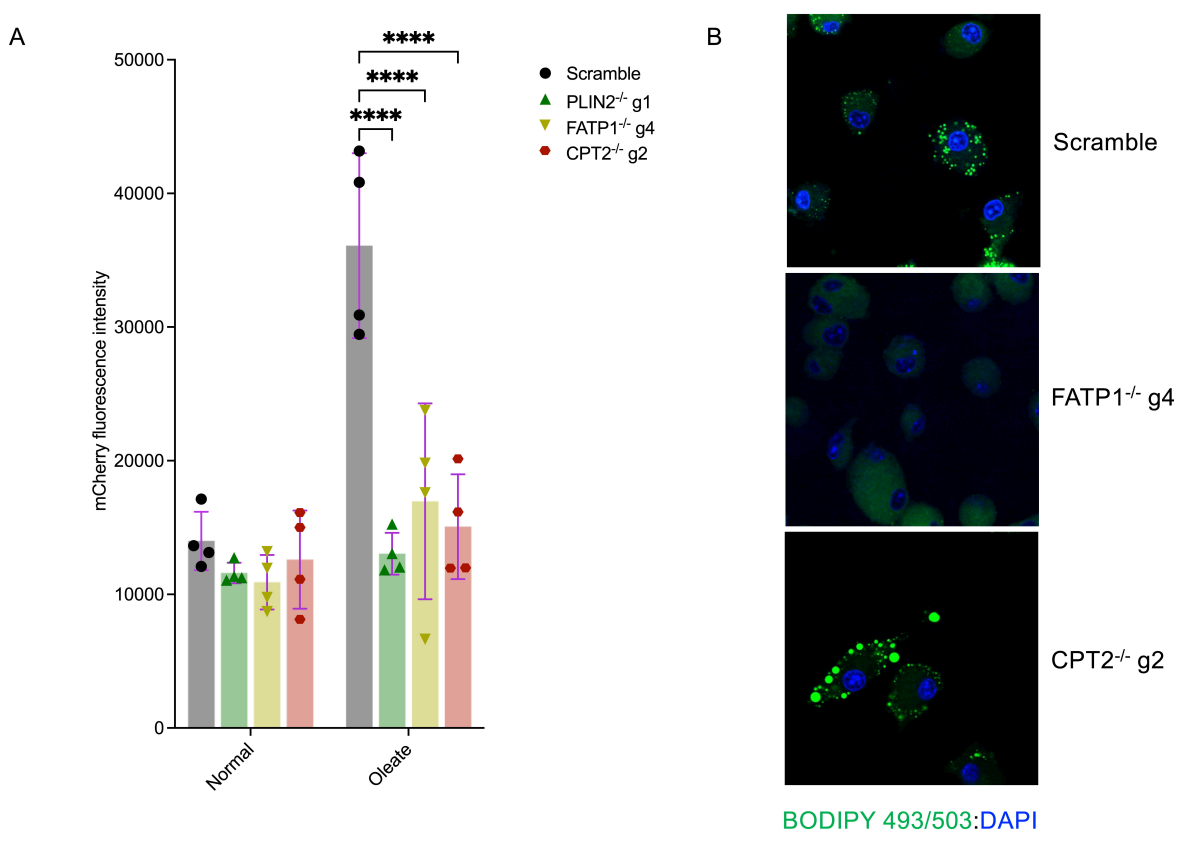
A
B
****
****
****
Scramble
PLIN2-/- g1
FATP1-/- g4
CPT2-/- g2
mCherry fluorescence intensity
50000
40000
30000
20000
10000
0
Normal
Oleate
Scramble
FATP1-/- g4
CPT2-/- g2
BODIPY 493/503:DAPI

A

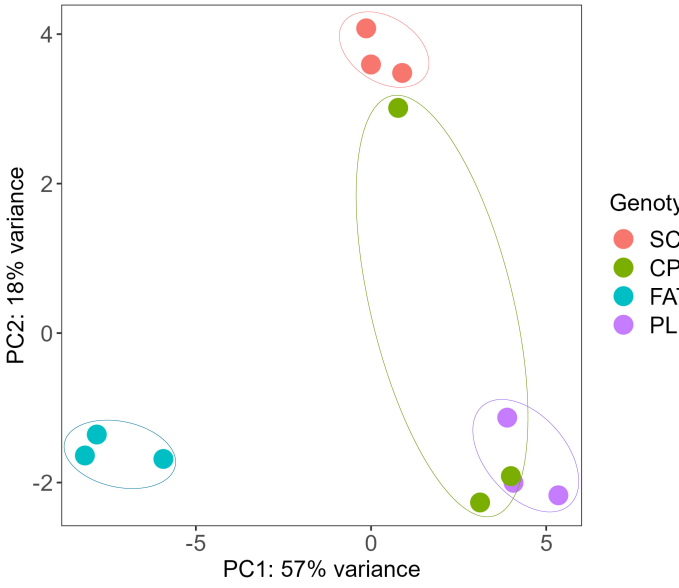
4
2
0
-2
-5
0
5
PC2: 18% variance
PC1: 57% variance
Genotype
SCmouse
CPT2komouse
FATP1komouse
PLIN2komouse

B

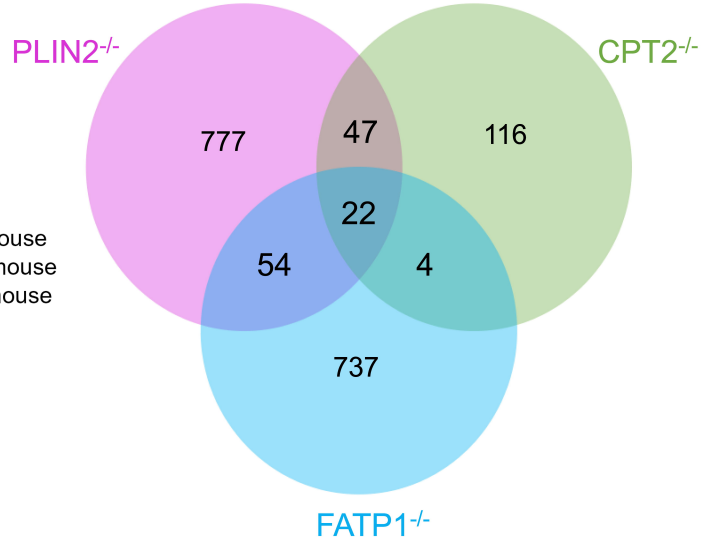
PLIN2-/-
CPT2-/-
FATP1-/-
777
47
116
22
54
4
737

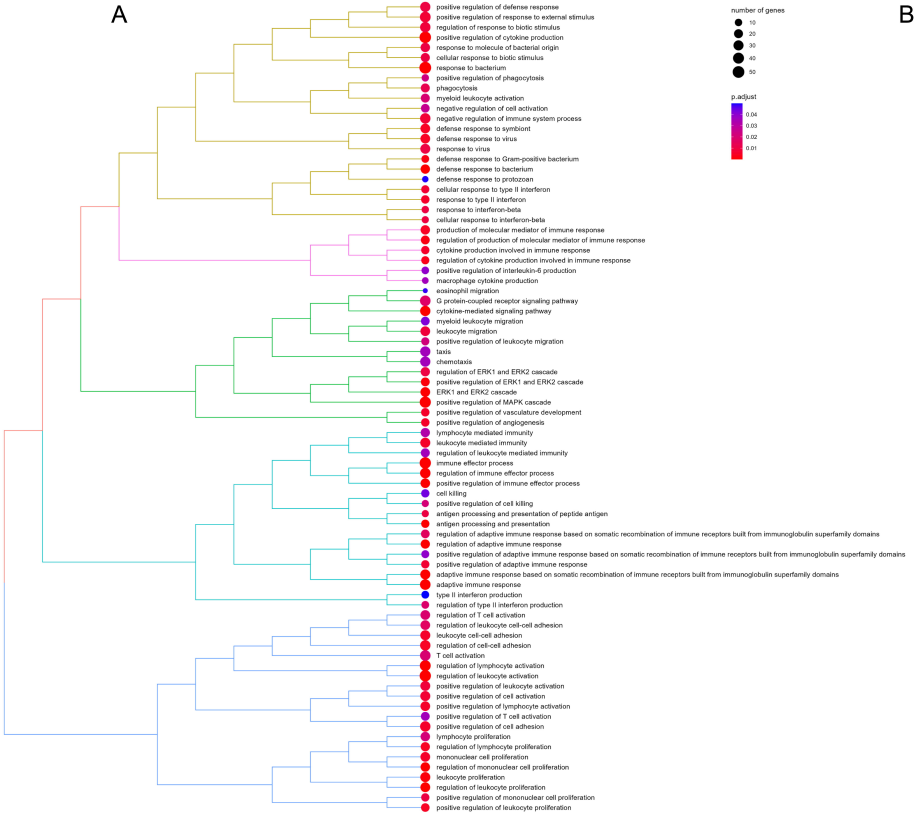

FATP1$^{-/-}$ up

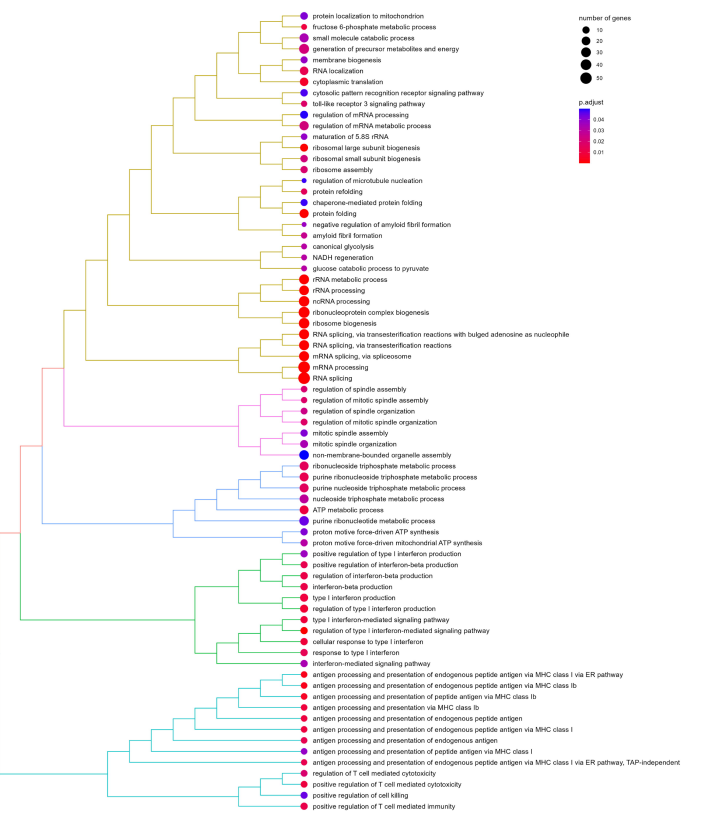

PLIN2$^{-/-}$ up

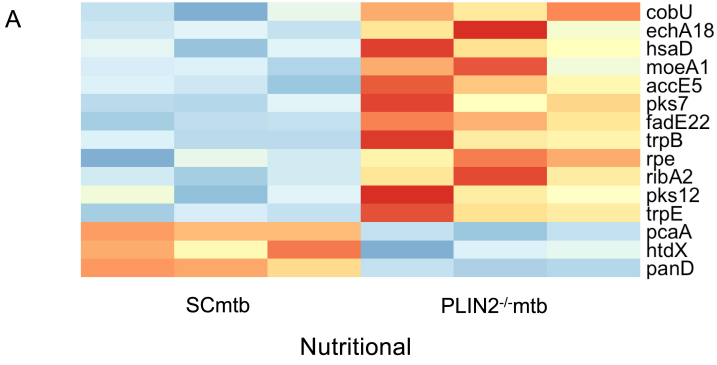
A
cobU
echA18
hsaD
moeA1
accE5
pks7
fadE22
trpB
rpe
ribA2
pks12
trpE
pcaA
htdX
panD
SCmtb
PLIN2-/-mtb
Nutritional

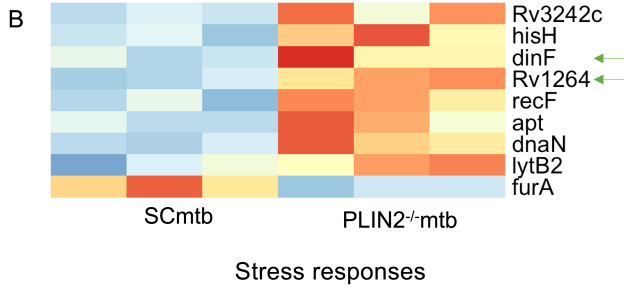
B
Rv3242c
hisH
dinF
Rv1264
recF
apt
dnaN
lytB2
furA
SCmtb
PLIN2-/-mtb
Stress responses

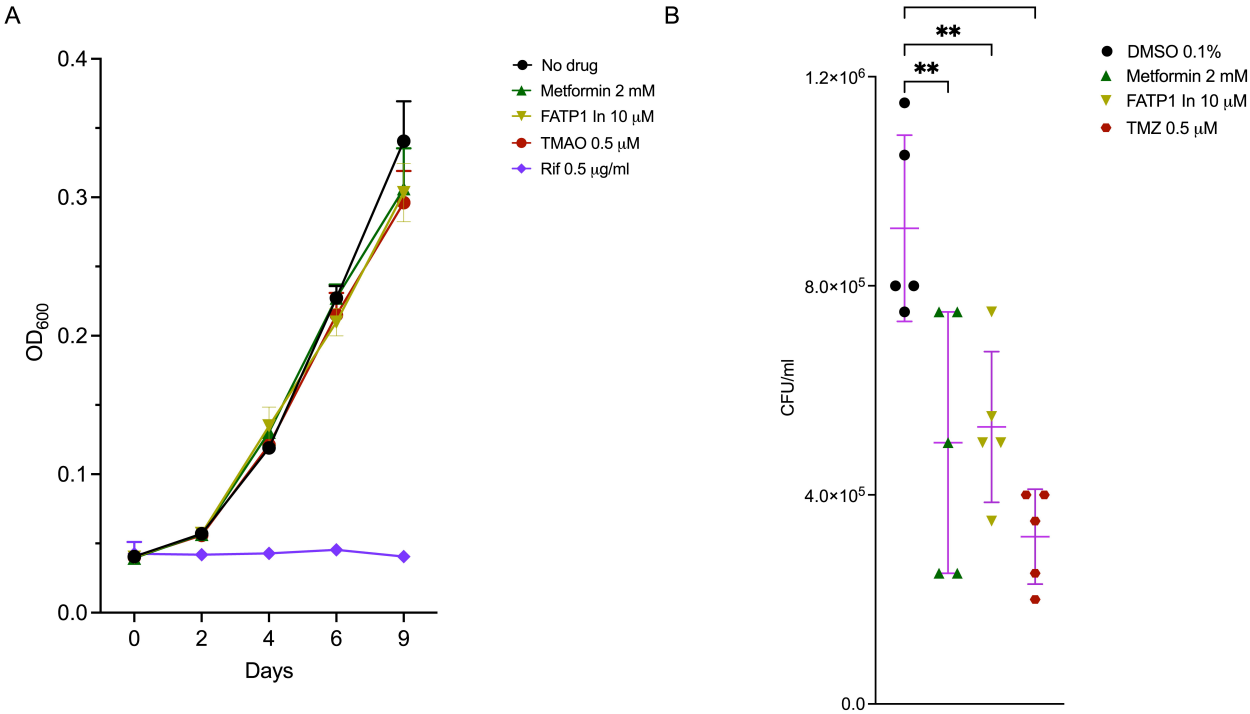
A
0.4
0.3
0.2
0.1
0.0
OD600
0
2
4
6
9
Days
No drug
Metformin 2 mM
FATP1 In 10 μM
TMAO 0.5 μM
Rif 0.5 μg/ml
B
****
**
**
1.2×10^6
8.0×10^5
4.0×10^5
0.0
CFU/ml
DMSO 0.1%
Metformin 2 mM
FATP1 In 10 μM
TMZ 0.5 μM